Ore Geology Reviews 114 (2019) 103143

Contents lists available at ScienceDirect

Ore Geology Reviews

journal homepage: www.elsevier.com/locate/oregeorev

Origin of the Xiaohekou skarn copper deposit and related granitoids in the Zha-Shan ore cluster area, South Qinling, China

Xiao Xiong, Laimin Zhu*, Guowei Zhang, Anlin Guo, Jun Zheng, Hang Jiang

State Key Laboratory of Continental Dynamics, Department of Geology, Northwest University, Xi'an 710069, China

ARTICLE INFO

Keywords:
Xiaohekou skarn Cu deposit
Thickened lower crust
Oxygen fugacity
Enriched lithospheric mantle-derived magmas
Qinling intracontinental orogeny

ABSTRACT

The Xiaohekou copper deposit is one of the few typical skarn-type, commercial deposits in the Zha-Shan ore cluster area in the eastern part of South Qinling. The ore-related granitoids in the Xiaohekou mining district include a number of small plutons of granodiorite porphyry and granite porphyry, as well as numerous dykes. They are characterized by relatively low SiO_2 (65.9–73.3 wt%) and MgO (0.26–1.72 wt%) contents, variable Mg# (29.4–64.0) values, high K_2O (3.11–5.75 wt%) content and negligible δEu (1.00–1.15) values. The samples also exhibit depletion in Cr, Ni, Nb, Ta, and Ti content, and high Sr/Y (46.6–64.7) and La/Yb (17.0–25.0) ratios. These features are similar to those of high-K calc-alkaline adakite-like magma formed by partial melting of thickened lower crust in continental collision zones or intracontinental settings. The majority of the samples have T_{DM2}(Hf) of 1.5–1.2 Ga, corresponding to weakly negative $\varepsilon_{Hf}(t)$ values (−4.75 to −0.13) typical of crustal material, but more than one quarter have T_{DM1}(Hf) of 0.80–0.71 Ga, corresponding to positive $\varepsilon_{Hf}(t)$ values of +0.07 to +2.45, indicating that the granitoids resulted from partial melting of Mesoproterozoic lower crustal rocks with significant input from enriched lithospheric mantle-derived magmas. Zircons from the Xiaohekou granitoids have ΔFMQ values concentrated around −0.62 to +5.54, most of which show the magma fO_2 of FMQ to HM, in accordance with the widespread occurrence of magnetite, hematite and specularite in the Xiaohekou skarn system, which is an indicator of relatively high fO_2 for a magmatic–hydrothermal system. The granitoids exhibit similar or even higher Ce^{4+}/Ce^{3+} (average of 452) and Eu/Eu* (average of 0.72) values in comparison with those of fertile Cu deposits worldwide, indicating that the Xiaohekou granitoids may possess the potential to form a large magmatic–hydrothermal Cu deposit. Zircons of the granitoids show obvious positive correlations between oxidation indices (Ce and Eu anomalies, Ce^{4+}/Ce^{3+} ratios, and ΔFMQ values) and $\varepsilon_{Hf}(t)$ values, implying the involvement of an oxidized mantle component which might have caused the fO_2 elevation and played an important role in the formation of Cu deposits. The zircon U–Pb ages (141.3 ± 1.3 and 138.1 ± 2.0 Ma) of the Xiaohekou ore-related granitoids obtained in this study are similar to the zircon U–Pb and molybdenite Re–Os ages yielded from porphyry Mo mineralization at the Chigou and Lengshuigou deposits in the Zha-Shan ore district, indicating that they are possibly part of a single tectonic, magmatic, and metallogenic event in the Yanshan orogeny. The ore-related granitoids in the Xiaohekou area were formed in a post-collisional compression–extension transition regime during the Early Cretaceous Qinling intracontinental orogeny. The orogeny can be attributed to the far-field effect of a switch from pre-Mesozoic Tethyan tectonics to Late Mesozoic Pacific tectonics. This triggered a stress field transition from N–S to E–W trending and from intracontinental subduction thickening to large-scale lithospheric delamination and thinning.

1. Introduction

The E–W-trending Qinling Orogen is sandwiched between the North China Block (NCB) and the South China Block (SCB) and links the Dabie Mountains to the east and the Qilian and Kunlun Mountains to the west (Fig. 1A) (Ames et al., 1996; Zhang et al., 2001; Dong and Santosh, 2016). Detailed investigations have shown that the Qinling Orogen represents a composite orogenic belt, which underwent four major episodes of accretion and collision between different continental blocks, including the subduction/accretion Grenvillian orogeny along the northern SCB, Paleozoic orogeny along the Shangdan suture, Triassic collisional orogeny along the Mianlue suture zone, and Late Mesozoic to Cenozoic intracontinental orogeny (Dong and Santosh, 2016). Accompanying the intracontinental orogeny, a major event of tectonics,

* Corresponding author.
E-mail address: zhulaimin@nwu.edu.cn (L. Zhu).

https://doi.org/10.1016/j.oregeorev.2019.103143
Received 16 December 2018; Received in revised form 5 September 2019; Accepted 27 September 2019
Available online 28 September 2019
0169-1368/ © 2019 Elsevier B.V. All rights reserved.

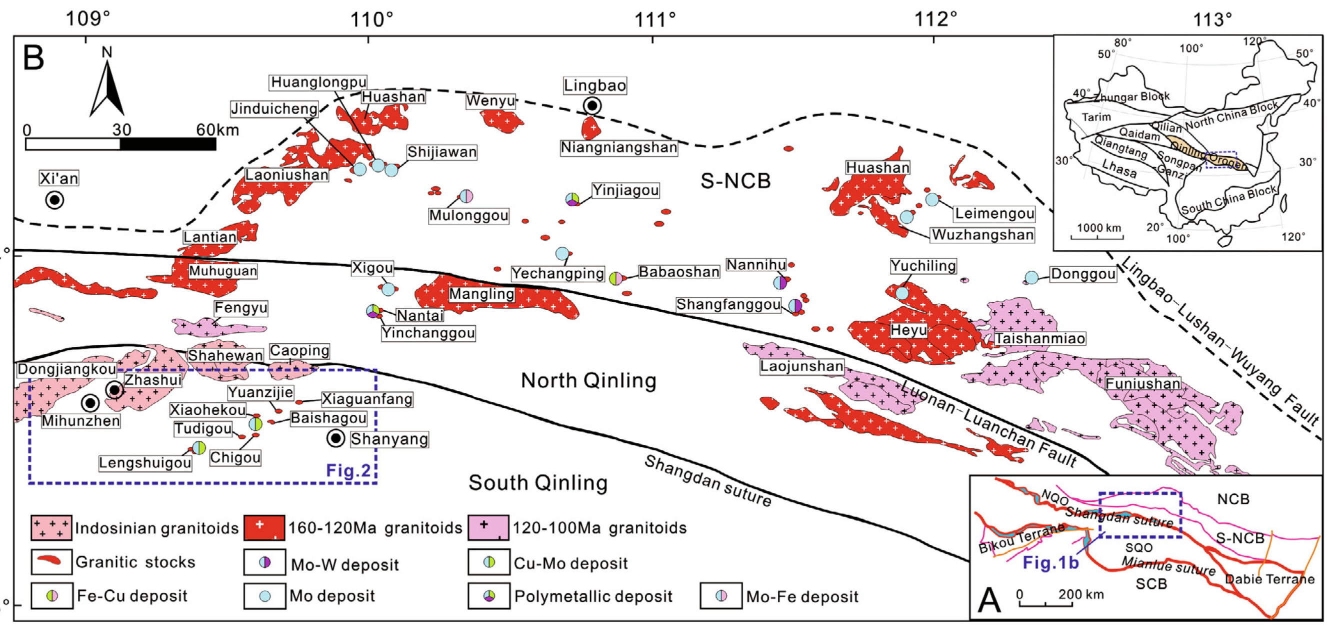

Fig. 1. Geological map of the Qinling Orogen, showing the distribution of the Mesozoic granitoids and major deposits (Modified after Wang et al., 2015a).

magmatism and metallogeny occurred in the Qinling Orogen, which makes the Eastern Qinling Orogen along the southern margin of the NCB (S-NCB, Fig. 1B) the most important molybdenum repository in the world, with 8.43–8.9 Mt of Mo and > 90% of Mo metal resourced from granitic stock-related porphyry and porphyry–skarn deposits aged 160–105 Ma (Stein et al., 1997; Li et al., 2007b, 2018; Mao et al., 2008, 2011; Zeng et al., 2013). Previous investigations mainly focused on geological and geochemical characteristics, precise ages, and tectonic settings of these deposits in the S-NCB (e.g., Stein et al., 1997; Chen et al., 2000; Zhu et al., 2010; Mao et al., 2008, 2011; Li et al., 2012a,b,c; Wang et al., 2011a, 2015a; Yang et al., 2012, 2015; Bao et al., 2014; Deng et al., 2017; Guo et al., 2018). Only a few magmatic-hydrothermal ore deposits have been identified in the Zha-Shan (Zhanshui and Shanyang Counties, Shaanxi Province) area, in the South Qinling Orogen (SQO) (Fig. 1B and 2), and research related to these deposits has only rarely been reported (Xie et al., 2017).

In recent years, comprehensive investigations including geology, large-scale geological mapping, geochemical anomaly, remote sensing, high-precision magnetic scanning and controlled source magnetotelluric surveys in the Zha-Shan ore cluster area carried out by the Northwest Mining and Geological Exploration Bureau for Nonferrous Metals have resulted in the discovery of Cu-Mo-Au orebodies in the Late Jurassic–Early Cretaceous Chigou–Lengshuigou porphyries and their contact zones. The intensive Late Jurassic–Early Cretaceous magmatic activity also resulted in the formation of a number of granitoids in the form of small hypabyssal intrusions such as the Xiaohekou, Lengshuigou, Chigou, Baishagou, Shuangyungou, Tudigou, Xiaguanfang and Yuanzijie granitic stocks in the Zha-Shan area (Zhang et al., 1989; Li et al., 2011; Ren et al., 2014; Chen et al., 2014; Yan et al., 2014; Xie et al., 2012, 2015, 2017; Wang et al., 2015b) (Fig. 2). Several mineralized hydrothermal alterations and porphyry–skarn Cu, Mo, Au, and Fe occurrences were discovered within the granitoids or locations nearby (Yan et al., 2014; Liu et al., 2014; Wang et al., 2015b; Xie et al., 2015). Thus, the Zha-Shan ore cluster area has been considered to be another potential target for the Late Mesozoic porphyry–skarn deposit exploration in the Qinling Orogen (Ren et al., 2014; Wang et al., 2015b).

The Xiaohekou and Lengshuigou Cu deposits are two of the few commercial deposits that have been mined in the Zha-Shan ore cluster area (Fig. 2). Studies of petrology, geochemistry and zircon U–Pb and molybdenite Re–Os chronology on the Lengshuigou porphyry–skarn deposit have recently been conducted (Xie et al., 2015, 2017). Although the Xiaohekou Cu deposit was discovered during the 1970s, the degree of geological research is still low at present – petrological and zircon U–Pb chronological study on the granitoids in the Xiaohekou mine are available only in Chinese publication (e.g., Zhang et al., 1989; Wu, 2013). Information on deposit geological characteristics, the genesis of mineralization-associated intrusions and the evaluation of metallogenic potential for the Xiaohekou deposit are still lacking. In recent years, magma oxygen fugacity (fO_2) have been advocated to be one of the key factors controlling the magmatic–hydrothermal mineralization (e.g., Carroll and Rutherford, 1987; Meinert, 1992; Ballard et al., 2002; Richards, 2003; Mengason et al., 2011; Trail et al., 2012; Sun et al., 2013, 2015; Dilles et al., 2014), because elevated fO_2 can destabilize sulfides and release chalcophile elements (e.g., Cu and Au) to the interacting fluid/melt/supercritical fluid (Richards, 2003; Jugo et al., 2010; Botcharnikov et al., 2011; Wilkinson, 2013). Zircon is ubiquitous in most calc-alkaline intrusions and resistant to subsolidus alteration. Thus, the zircon Ce^{4+}/Ce^{3+} ratio and ΔFMQ value have become useful tools for evaluating the economic potential of porphyry–skarn Cu-–Mo–Au mineralization (e.g., Ballard et al., 2002; Liang et al., 2006; Trail et al., 2012; Wang et al., 2013a, 2015c; Xu et al., 2016; Cao et al., 2018).

In this study, we carry out detailed geological study of the Xiaohekou skarn Cu deposit and present the integrated analyses of in situ U–Pb dating, Hf isotope, and trace element (Ti, Th, U, Hf, and rare earth elements) data from zircons and rock major and trace element geochemistry of mineralization-related intrusions. We first aim to constrain the timing, source, petrogenesis, and mechanism of Cu enrichment in granitoids of the Zha-Shan ore cluster area. The other aim of this work is to establish prospecting criteria of fO_2 for distinguishing between fertile and barren granitoids in the Zha-Shan ore cluster area.

2. Geologic background

The tectonic framework of today's Qinling Orogen is composed of three crustal units separated by two suture zones (Fig. 1). From north to south, these are the S-NCB, the Shangdan suture zone, the South Qinling Orogen (SQO), the Mianlue suture zone, and the N-SCB (Zhang et al., 2001; Dong and Santosh, 2016). A brief overview focusing on the SQO is given below.

Situated between the Shangdan Tectonic Zone to the north and the

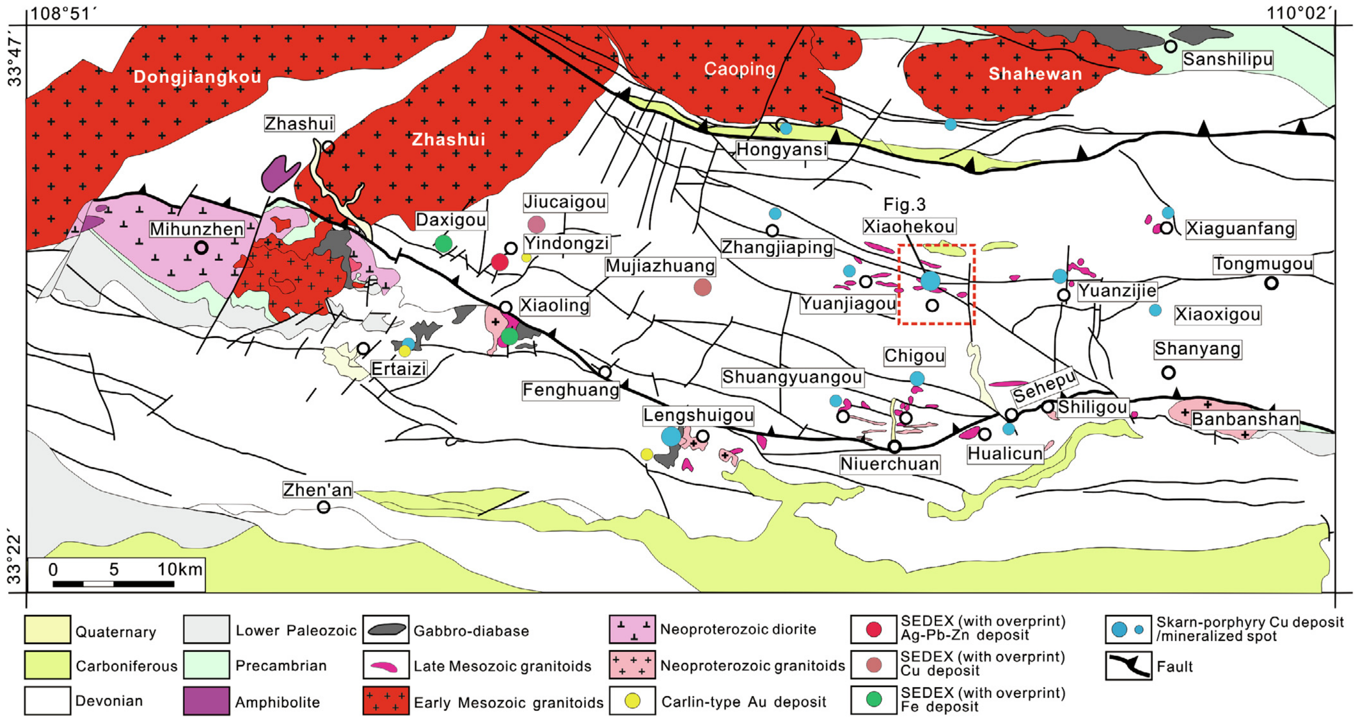

Fig. 2. Geological map of the Zha-Shan ore district cluster showing the distribution of granitoids and mineralization (modified after Wu et al., 2014).

Mianlue suture zone to the south, the SQO is characterized by a series of south-vergent thrusts and folds of an imbricated thrust–fold system (Zhang et al., 2001). The basement, as represented by the Douling and Xiaomoling Complexes and the Wudang and Yaolinghe Groups, is dominated by the Neoproterozoic volcano-sedimentary assemblages that were deposited in rift-type or subduction-related basins and metamorphosed under greenschist facies conditions (Ling et al., 2008). Recent geological and chronological studies have detected a series of Neoproterozoic basement terrains with mafic to felsic intrusive rocks in the middle and western segments of the SQO, such as the Mihunzhen and Lengshuigou intrusions (Fig. 2), constituting an E–W-trending Neoproterozoic uplift zone (Hu et al., 2016). The sedimentary cover includes Sinian clastics and carbonate rocks, Cambrian–Ordovician limestones, Silurian shales, and Devonian to Carboniferous clastic rocks and limestones. A few remnants of the Upper Paleozoic–Lower Triassic clastic sedimentary rocks are also distributed across the northern part of the SQO (Zhang et al., 2001).

Sedimentary strata in the Zha-Shan ore cluster area mainly comprise 6800- to 18,000-m-thick Devonian Liuling Group and Lower Carboniferous Eryuhe Formation (Fig. 2). The Liuling Group comprises marine clasitic-carbonate-barite strata and a greenschist facies of sandstone, siltstone, and shale, along with minor conglomerate units, and is divided from bottom to top into Middle Devonian Niuerchan, Chigou, and Qingshiya Formations and Upper Devonian Xiadonggou and Tongyusi Formations, all of which were deposited in an active continental margin setting (Yan et al., 2012). Several large SEDEX-type (or later overprinted by tectono-hydrothermal processes) Cu–Ag–Pb–Zn–Fe deposits (e.g., Daxigou, Yindongzi, and Mujiazhuang; Fig. 2) were hosted in the Devonian Qingshiya Formation (Wang et al., 2010; Liu et al., 2015; Zhan et al., 2019). Three magmatism stages are recognized in the Zha-Shan ore cluster area, i.e., the Late Neoproterozoic (878–635 Ma), Late Triassic (225–210 Ma) and Late Mesozoic (150–140 Ma) (Fig. 2). Late Neoproterozoic magmatism appeared sparsely along the Shanyang–Fengzhen Fault and is presented by Lijiabian diabase-gabbro, Banbanshan potash granite, and Lengshuigou quartz diorite + albitite + granite (Wu et al., 2012; Xie et al., 2017). Large Triassic granitic batholiths (Dongjiangkou, Zhashui, Shahewan, and Caoping) are exposed to the northwest of the Zha-Shan area and mainly comprise rapakivi, monzogranite porphyry, and granodiorite porphyry (Li et al., 2015 and references therein). The Devonian Chigou, Qingshiya, and Xiadonggou Formations are the main hosts for porphyry-skarn Cu (Mo) systems and Late Mesozoic granitoids within the Zha-Shan district. These units are overprinted extensively by hornfels and skarn alternating along the contact between the Xiaohekou, Yuanjiagou Chigou, Shuangyuangou, Tudigou, Yuanzije, Xiaguanfang, Baishagou, and Lengshuigou granitic stocks and Devonian strata (Fig. 2). These granitic stocks are composed dominantly of high-K calc-alkaline I-type diorite to granodiorite porphyry with minor granite porphyry (Wu, 2013; Wang et al., 2015b; Ren et al., 2014; Yan et al., 2014; Xie et al., 2015, 2017), and accompanied by minor amounts of cryptoexplosion breccia (Wang et al., 2010).

3. Geology of the Xiaohekou Cu deposit

3.1. General ore geology

The Xiaohekou skarn Cu deposit contains more than 0.05 Mt of proven Cu reserve. It is located at the central Zha-Shan polymetallic ore cluster area of east South Qinling (Figs. 1 and 2) in northwest Shanyang County, Shaanxi Province. The deposit is bounded by the Hongyansi–Heishan fault to the north and the Shanyang–Fengzhen fault to the south (Fig. 2). Structurally, several NW-, NNE-, and NS-trending faults cross cut the area. The local stratigraphy at the Xiaohekou skarn Cu deposit is simple, being dominated by low-grade metamorphic sedimentary rocks of Devonian Qingshiya ($D_{2\text{-}3}q$) and Tongyusi (D_3ty) Formations (Fig. 3). The Devonian Qingshiya Formation crops out in the south of the mining district and is composed of slate, phyllite, and limestone, interlayered with one another. The Devonian Tongyusi Formation, comprising phyllitic slate–metasiltstone interbeds and carbonate rocks, is distributed in the north. Orebodies in the deposit are generally hosted by carbonate and marble (Figs. 3, 4, and 6). These strata appear in north-dipping monoclinal attitude dipping at angles of 40° to 54°. The ore district is controlled by the regional Zhangjiaping–Yuanjiagou–Xiaohekou–Yuanzijie–Tongmugou Fault (Yan et al.,

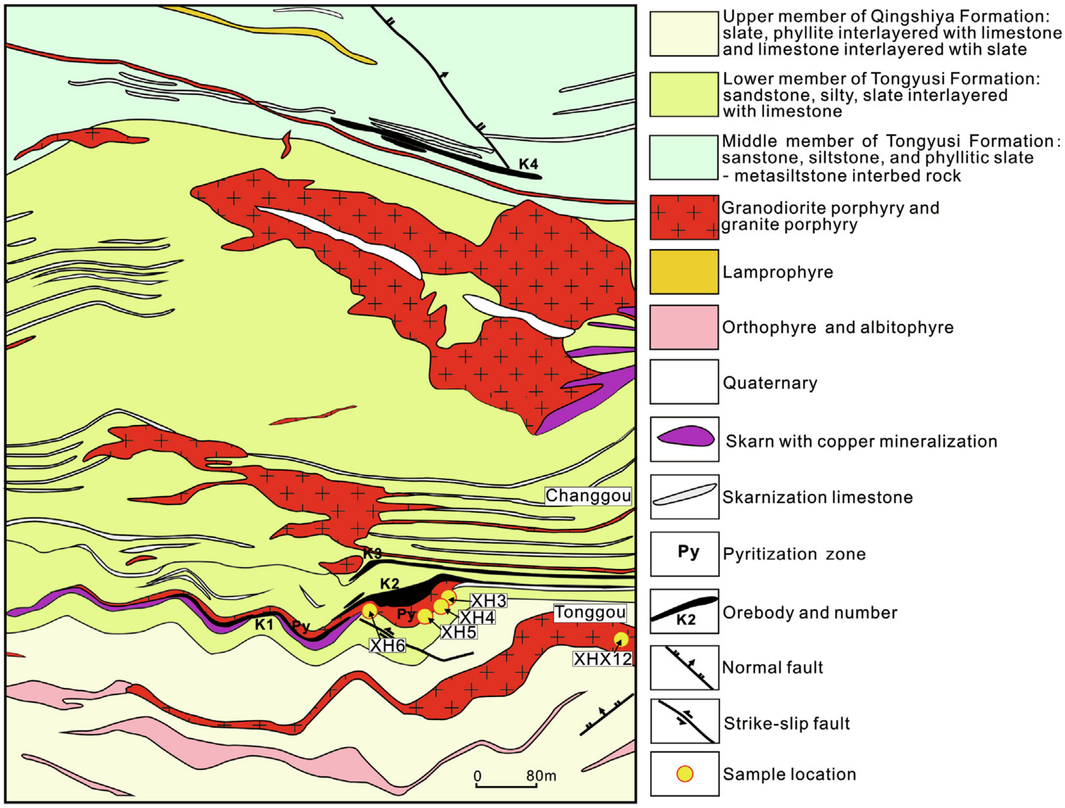

Fig. 3. Map of the Xiaohekou area in the Zha-Shan ore district cluster (modified after Shaanxi Mineral Resources and Geological Survey, 2013).

2014) and cut by NW-trending sinistral strike–slip faults. The Xiaohekou granitoids intrude into the intersections of these faults (Figs. 2 and 3). Most orebodies were developed in interlayered shear or fracture zones near the contacts between granitoids and strata (Fig. 4).

3.2. Alterations and mineralization stages

Wall rocks in the Xiaohekou skarn Cu deposit have experienced various types of strong alteration. Skarn-style alteration, silicification, and carbonatization are widely developed in exo-contact zones between granitoids and Devonian strata of the Tongyusi Formation (Fig. 6). Cu mineralization is spatially and temporally associated with pervasive skarn-type alteration zones (Fig. 4), which produce calc-silicates including prograde and retrograde skarn assemblages. The prograde skarn is mainly composed of anhydrous skarn (e.g., garnet and diopside) minerals (Figs. 5 and 6B, E, I, G). The retrograde skarn (hydrous skarn) consists of actinolite, epidote, and chlorite, which were alteration products of early stage skarn minerals (Fig. 6B, F, and L). The skarn bodies occur between granitoids and marble (Figs. 3 and 4) and apparently show strata-bound characteristics. Gray and white massive marble lenses are commonly observed in skarn (Fig. 6D) and dominated by fine- to medium-grained recrystallized calcite, with abundant ore sulfides and minor chlorite, quartz, and talc, displaying in granoblastic texture. Silicification is characterized by polymetallic sulfide-bearing quartz veinlets that cut the skarn and marble (Fig. 6C). Carbonatization is represented by parallel calcite ± quartz veins, 1–30 cm wide and tens of meters long (Fig. 6E). The veins usually cut through the skarn.

In terms of ore fabrics, mineralogical assemblages, and crosscutting relationships, the mineralization of the Xiaohekou skarn Cu deposit can be divided into the following stages: (1) the anhydrous skarn stage, (2) the hydrous skarn–oxide stage, (3) the quartz–polymetallic sulfide stage, and (4) the carbonate–quartz stage (Fig. 5). The anhydrous skarn stage represents the earliest stage of hydrothermal activity and is characterized by the formation of anhydrous minerals, including garnet (> 70%) and diopside (< 30%) (Fig. 6B). Widely-seen garnets are reddish- or yellowish-brown (Fig. 6F and G) and display fine- to coarse-grained (0.3–1 mm) subhedral to euhedral crystals with significant zoning (Fig. 6J and K). Diopsides occur as short-column crystals or fine-grained anhedral granular aggregates (Fig. 6K and L). The hydrous skarn–oxide stage is defined by the occurrence of an assemblage of retrograde skarn minerals, such as actinolite, epidote, and chlorite (Fig. 6F and L), accompanied by abundant Fe oxides (e.g., magnetite and specularite). These minerals usually replaced the early anhydrous skarn minerals, specifically, the prograde garnet and diopside (Fig. 6F, G and H). The quartz–polymetallic sulfide stage is the main Cu mineralization stage, including the deposition of chalcopyrite, pyrite, pyrrhotite, bornite, molybdenite, and quartz (Fig. 6C). These sulfides typically surround garnet, fill the fractures in skarn (Fig. 6I and M), or cut the skarn and magnetite as veins, indicating that the Cu mineralization occurred later than stages (1) and (2). Calcite and quartz mark the final stage, with minor deposition of bornite, pyrite, and chalcopyrite. These minerals occur as veins crosscutting the early skarns and quartz–polymetallic sulfide veins (Fig. 6E) or filling interstices and intergranular spaces of skarn and metallic minerals (Fig. 6J and P)

3.3. Orebodies and mineralogy

A total of 10 economic orebodies have been detected in the deposit and all of them were developed in the skarn and marble in exo-contact zones of granitoids. Orebodies are stratiform, stratoid, lenticular, and vein-like that are north-striking with dips of 48°–55°, and generally parallel to the strata (Fig. 4). The orebodies have lengths of 63–336 m and varied thicknesses of 0.66–3.27 m, are continuously distributed and extend 24–75 m downward. They pinch out in the skarn or marble. The orebodies are mainly Cu orebodies with a grade of 0.85% to 3.62% Cu, followed by Cu–Fe orebodies. Metallic mineral compositions are complex and predominantly chalcopyrite, pyrite, magnetite, pyrrhotite, molybdenite, specularite, and hematite, with minor marcasite,

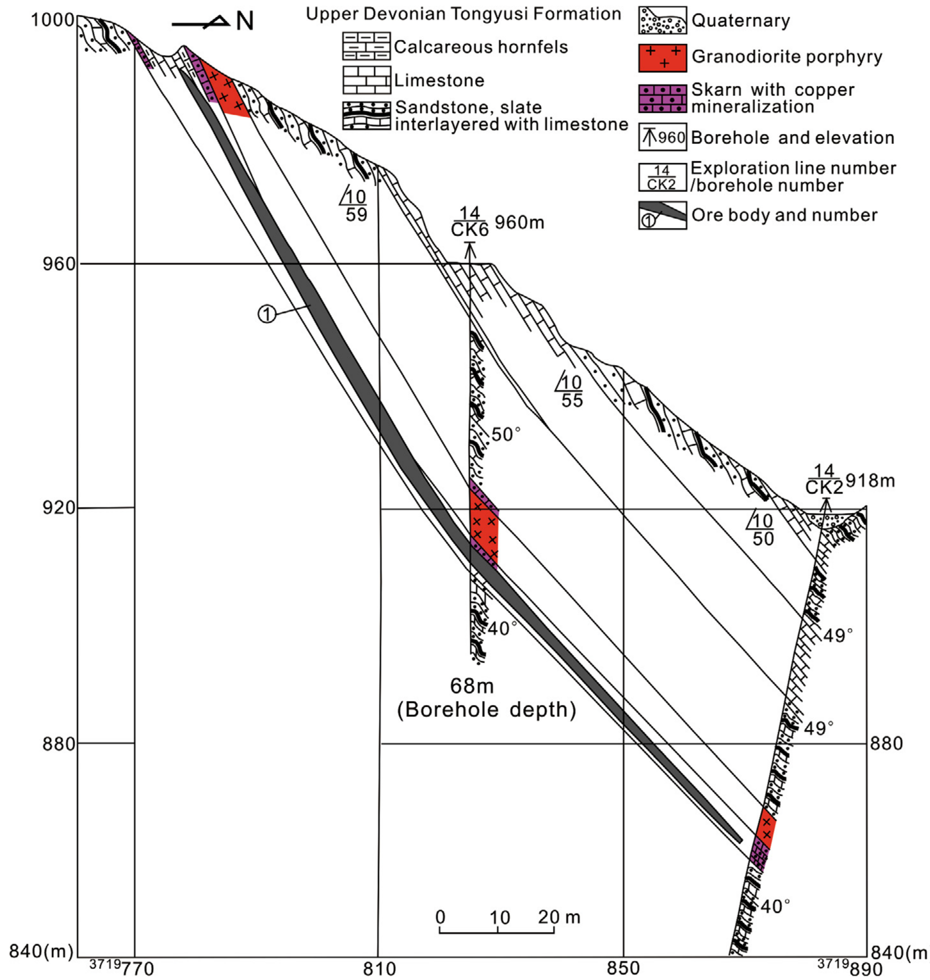

Fig. 4. Geologic cross section through the Xiaohekou skarn Cu deposit, showing the spatial relationships among strata, intrusions, skarn and orebodies (modified after Shaanxi Mineral Resources and Geological Survey, 2013).

sphalerite, galena, siderite, chalcocite, and electrum. Associated gangue minerals include garnet, diopside, feldspar, actinolite, epidote, chlorite, quartz and calcite (Fig. 6).

According to ore mineral assemblage, ores can be subdivided into three subtypes, as follows: (1) Chalcopyrite ores, the most important Cu-bearing mineral in the Xiaohekou mining district, occur as massive and disseminated subhedral grains with other sulfides (including pyrite, molybdenite, and minor pyrrhotite, sphalerite, and galena) in quartz veins. The ores also can be seen in the intergranular spaces of garnet and diopside and replace garnet (Fig. 6I and M). Molybdenite, as a by-product, occurs as fine flake aggregates and thin veins in diopside–-garnet skarn (Fig. 6O). (2) Cu-bearing pyrrhotite ores (Fig. 6N), with a grade of > 2.0% Cu, exist in diopside and diopside–garnet skarns. The main metallic minerals include chalcopyrite and pyrrhotite, followed by pyrite and galena. Anhedral chalcopyrite and pyrrhotite commonly wrap euhedral pyrite, showing typical poikilitic texture. These ores occur in the forms of massive aggregates, dense disseminations, and veinlets with widths of 0.3–0.8 cm. (3) In Cu-bearing magnetite ores, magnetite forms the earliest and replaces skarn minerals showing a metasomatic relict texture (Fig. 6G). Chalcopyrite and pyrite commonly occur as disseminated spots distributed in magnetite or as a banded structure distributed parallel to magnetite. This type of ore is characteristic of a magnetite + chalcopyrite + pyrite assemblage, which usually occur in bands intercalated with garnet in skarn.

3.4. Lithology of the granitic intrusions at the deposit

Compared with the country rocks, granitic intrusions are generally fresh with only slight hydrothermal alteration. Detailed field and petrographic studies illustrate that intrusive rocks in the Xiaohekou mining district are of granodiorite porphyry and granite porphyry. The intrusive rocks are mainly exposed in E–W-trending belts and are present as small apophyses and dykes with widths not more than 0.2 km and lengths of 0.7–1.0 km, intruding the Tongyusi (D_3ty) and Qingshiya ($D_{2-3}q$) Formations (Fig. 7B). Granodiorite porphyry, the main rock type in the area, has an off-white color, porphyritic texture and massive structure (Fig. 6A and 7C). Phenocrysts are euhedral plagioclase (15–20%), amphibole (5–10%), subhedral quartz (< 5%), and minor K-feldspar (< 3%) and biotite (< 3%), with sizes of 0.3–2 mm (Fig. 7E–G). The matrix exhibits fine-grained granular and felsitic textures, consisting of 20–25% plagioclase, 10–15% K-feldspar, 5–10% amphibole, and 5–8% quartz. Accessory minerals include apatite, sphene, zircon, and magnetite. Granite porphyry has a pale red color, a massive structure, and a porphyritic texture (Fig. 7D). Phenocrysts are euhedral lath-shaped K-feldspar (5–10%), with sizes of 0.5–2 mm, and euhedral to subhedral quartz (5–10%) with hexagonal bipyramid texture, with sizes of 0.5–1.5 mm (Fig. 7H and I). The matrix exhibits a fine-grained texture and is composed of K-feldspar (30–40%), plagioclase (30–35%), quartz (25–30%), and biotite (< 5%).

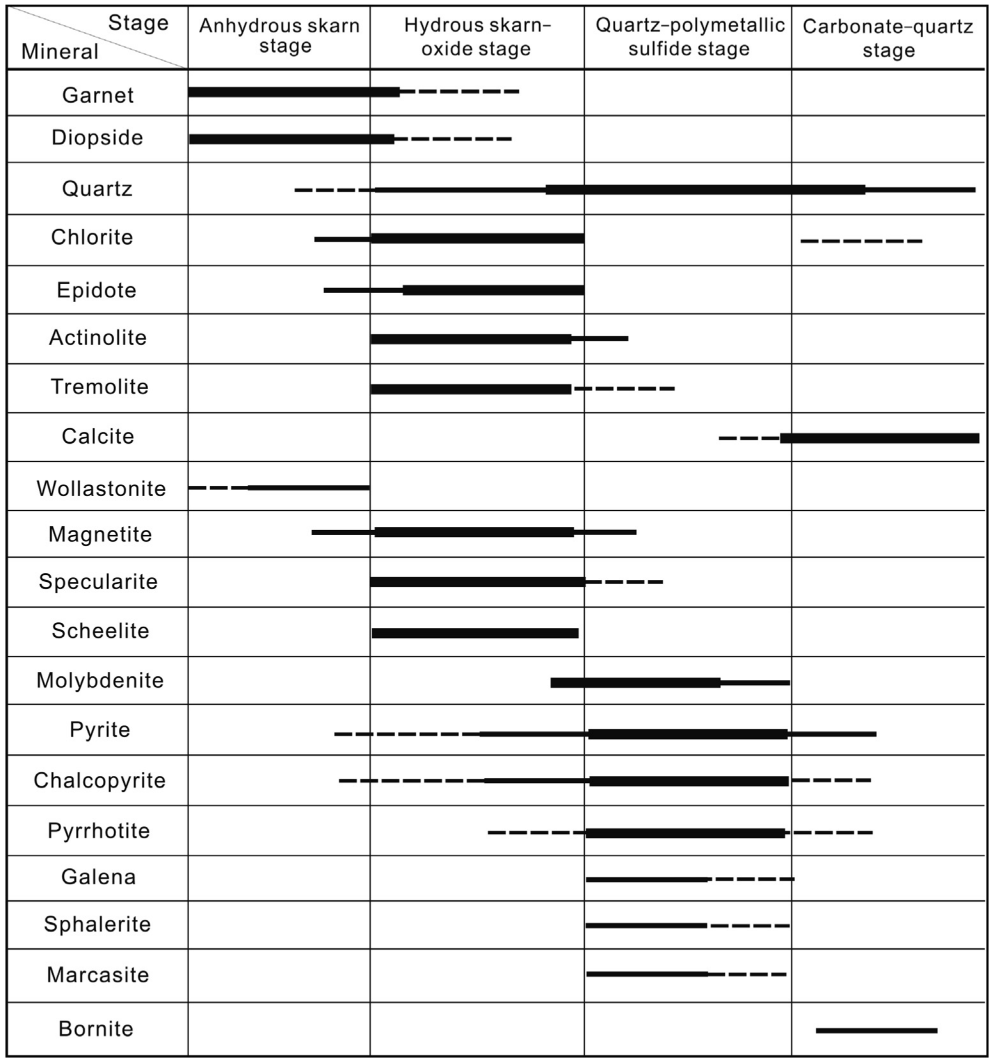

Fig. 5. Mineral paragenesis for the Xiaohekou Cu deposit.

4. Sampling and analytical methods

In the Xiaohekou mining district, five samples of granitic intrusions were collected from both underground tunnels at 860 m depth, and from the surface. Samples XH3, XH4, XH5, and XH6 are from granodiorite porphyry. Sample XHX12 is granite porphyry (Table ES1).

4.1. Major and trace elements

The fresh portions of whole-rock samples were cleaned, powdered to < 200-mesh using a crusher machine made of tungsten carbide and then dried for analysis. Major and trace elements were measured at the Key Laboratory of Continental Dynamics of Northwest University, Xi'an, China. Major oxides were determined by using X-ray fluorescence (RIX2100X sequential spectrometer) on fused Li-borate glass beads, with BCR-2 and GBW07105 as reference materials. For trace element analysis including rare earth elements (REE), sample powders were loaded into high-pressure Teflon bombs, with HF + HNO_3 mingling added. The bombs were put into a stainless steel sleeve for digestion at 190 °C for 48 h. Trace and REE elements were analyzed using an Agilent 7500a ICP-MS. The standards BHVO-2, AGV-2 and BCR-2 were used for analytical control.

4.2. Zircon U–Pb age and trace elements

Two representative samples XH5 and XHX12 were selected for in-situ zircon U-Pb, trace elements, and Lu-Hf isotope analyses. These analyses were performed at the State Key Laboratory of Continental Dynamics, Northwest University, Xi'an, China. Zircon grains were extracted by heavy liquid and magnetic separation techniques, and handpicked under a binocular microscope. They were mounted in epoxy blocks and polished to obtain a smooth surface, and then cleaned using 3% HNO_3 to remove lead contamination prior to LA-ICP-MS analysis. Cathodoluminescence (CL) images were taken on a Quanta 400 FEG scanning electron microscope from FEI (USA8) equipped with a Mono CL3+ cathodoluminescence spectroscope. Zircon U–Pb ages and trace elements were obtained using a GeoLas 2005 Laser Ablation (Coherent, USA) coupled to an Agilent 7500a ICP-MS. The diameter of the laser ablation crater was 32 μm. The detection limits of zircon trace elements are generally < 0.01 ppm. According to the reflected light and CL images (Fig. 10), we chose zircons with similar oscillatory zones avoiding cracks and tiny inclusions as far as possible. Harvard zircon 91,500 and GJ-1 were used as the external calibration standards and silicate glass NIST SRM610 as a standard to calculate element concentrations. The GLITTER 4.4 V program (Jackson et al., 2004) was used for processing acquired data. The U-Pb ages were calculated using ISOPLOT 3.0 V (Ludwig, 2003). The detailed analytical methods are based on Yuan et al. (2004).

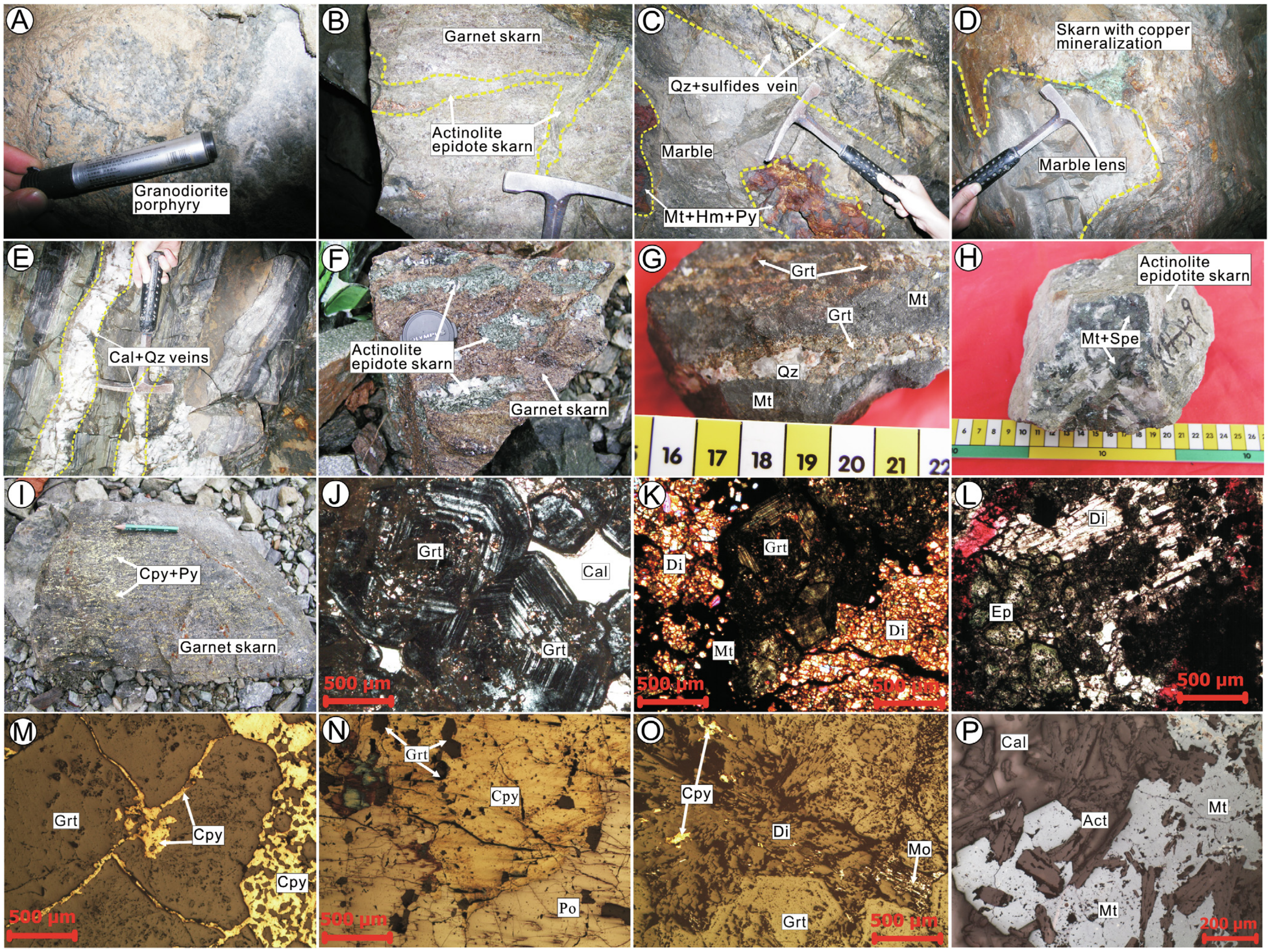

Fig. 6. Representative photographs and photomicrographs showing ore geology of the Xiaohekou skarn Cu deposit. **A** granodiorite porphyry in the underground tunnels at 860 m depth; **B and F** hydrous skarn overprinting anhydrous skarn; **C** quartz–polymetallic sulfide veins and massive magnetite + hematite + pyrite assemblage occurring in the marble; **D** marble lens in skarn; **E** barren carbonate–quartz veins in late stage; **G** magnetite + quartz replacing earlier garnet; **H** magnetite + specularite occurring in actinolite–epidote skarn; **I** chalcopyrite + pyrite veinlets in the garnet skarn; **J** calcite filling the intergranular spaces of garnet; **K** coexisting diopside and garnet are replaced by magnetite; **L** epidote replacing euhedral diopside crystal; **M** chalcopyrite replacing and filling in the cracks of garnet; **N** coexisting pyrrhotite + chalcopyrite replacing garnet; **O** chalcopyrite and molybdenite occurring in the diopside–garnet skarn; **P** magnetite replacing actinolite skarn. Grt-garnet, Di-diopside, Ep-epidote, Act-actinolite, Qz-quartz, Cal-calcite, Cpy-chalcopyrite, Py-pyrite, Po-pyrrhotite, Mt-magnetite, Hem-hematite, Spe-specularite, Mo-molybdenite.

4.3. Zircon Lu–Hf isotope

In-situ Lu–Hf analysis for zircons was carried out using the same laser system coupled with a Nu Plasma HR (Wrexham, UK) MC-ICP-MS. The instrumental conditions and data acquisition were described by Yuan et al. (2008). The analyses were conducted with a 44 μm ablation spot size. Harvard 91500 and GJ-1 were used as reference standards during analyses. The decay constant for ^{176}Lu of 1.867×10^{-11} yr^{-1} (Söderlund et al., 2004) and measured $^{176}Lu/^{177}Hf$ were used to calculate initial $^{176}Hf/^{177}Hf$ ratio. A chondritic reservoir with $^{176}Hf/^{177}Hf$ of 0.0336 and $^{176}Lu/^{177}Hf$ of 0.282785 (Bouvier et al., 2008) were used to calculate $\varepsilon_{Hf}(t)$ values. Single-stage Hf model ages (T_{DM1}) are calculated relative to the depleted mantle with a present-day $^{176}Hf/^{177}Hf$ ratio of 0.28325 and $^{176}Lu/^{177}Hf$ of 0.0384, and two-stage Hf model ages (T_{DM2}) are calculated by assuming a mean $^{176}Lu/^{177}Hf$ value of 0.015 for the average continental crust (Vervoort and Blichert-Toft, 1999).

5. Result

5.1. Whole-rock geochemistry

The major and trace element compositions of nine granitoid samples from the Xiaohekou intrusions are presented in Table ES1, of which the data of four samples are compiled from Wu (2013). The major element compositions have only a slight variation with medium SiO_2 (65.9–73.3 wt%) and Al_2O_3 (13.0–15.4 wt%) contents, high K_2O (3.11–5.75 wt%), $K_2O + Na_2O$ (5.84–8.95 wt%), and K_2O/Na_2O ratios (0.74–63.9, average of 6.08), and low P_2O_5 (0.06–0.28%) and TiO_2 (0.09%–0.48%) contents. These granitoids have MgO contents ranging from 0.26 wt% to 1.72 wt% (average of 1.02 wt%) and variable Mg# values ranging from 29.4 to 64.0 (average of 45.9). Fig. 8A and B show that the Xiaohekou intrusions are typical metaluminous to weakly peraluminous (A/CNK = 0.81–1.01, average of 0.95, except for sample XH3), similar to the high-K calc-alkaline I-type granites. The P_2O_5 contents decrease with SiO_2 increase (Fig. 8C), consistent with the I-type magma evolution trend (Chappell, 1999; Li et al., 2007a).

With a total REE concentration of 42.4–144 μg/g, the Xiaohekou granitoids display the chondrite-normalized REE distribution patterns

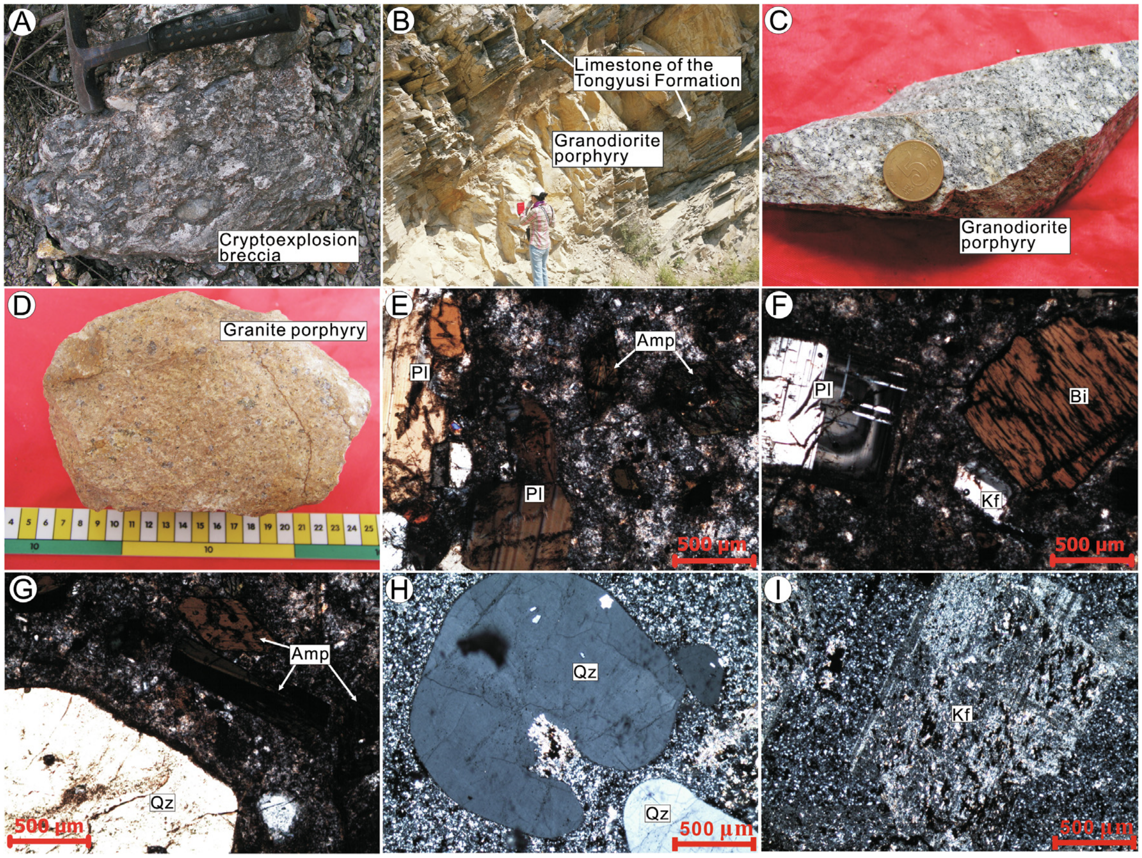

Fig. 7. Photographs and photomicrographs of the ore-related granitoids from the Xiaohekou skarn Cu deposit. **A** cryptoexplosion breccia in the ore district; **B** granodiorite porphyry dykes intruding into the Tongyusi (D_3ty) Formation; **C** granodiorite porphyry sample from the underground tunnels at 860 m depth; **D** granite porphyry sample; **E–G** plagioclase, amphibole, quartz, biotite, and K-feldspar phenocrysts of the granodiorite porphyry; **H and I** phenocrysts of subhedral–euhedral K-feldspar and quartz with hexagonal bipyramid texture in the granite porphyry. Pl-plagioclase, Amp-amphibole, Kf-K-feldspar, Bi-biotite, Qz-quartz.

characterized by right-inclined [LREE/HRRE = 6.9–13.4; $(La/Yb)_N$ = 5.60–17.1] enriched LREE and flat HREE patterns [$(La/Sm)_N$ = 3.50–5.30; $Gd/Yb)_N$ = 1.1–2.2] (Fig. 9A). Except for sample XH4 (δEu = 0.89), most of the granitoids yield weakly positive Eu anomalies (δEu = 1.00–1.15) (Fig. 9; Table ES1). On the mantle-normalized multielement diagrams (Fig. 9B), the Xiaohekou granitoids basically show no difference from one another with pronounced relative enrichment of Rb, Ba, U, Pb, and K and depletion of Ta, Nb, Sr, P, and Ti, similar to those of granite originating from the melting of ancient crust (Sun and McDonough, 1989). The rock samples (except for samples XH3 and XH4) yield high Sr/Y (46.6–64.7) and La/Yb (17.0–25.0) ratios and low Y and Yb contents (9.6–16.2 ppm and 0.95–1.75 ppm, respectively) (Table ES1; Fig. 13A,B), indicating that the Xiaohekou granitoids have adakitic affinities (Defant and Drummond, 1990; Moyen, 2009).

5.2. Zircon U–Pb ages and trace elements

The LA-ICP-MS zircon U–Pb dating results of 41 spots for 2 samples are summarized in Table ES2 and shown in Fig. 10. Most zircons are colorless or pale yellow, transparent and euhedral with columnar crystal forms and 100–400 μm in length. In representative CL images, most zircons exhibit clear oscillatory zoning.

Analyses of 21 spots from sample XH5 yield Th and U concentrations of 28.2–456 and 39.5–947 ppm, respectively, with the Th/U ratios of 0.21–1.16 (average of 0.47). A total of 15 analysis spots yield a

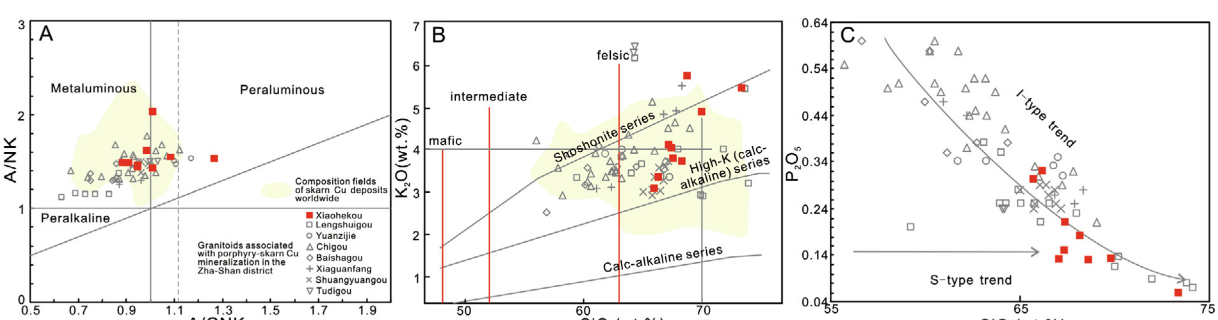

Fig. 8. A/NK vs. A/CNK (A, after Maniar and Piccoli, 1989), SiO_2 vs. K_2O (B, after Rollinson, 1993), and SiO_2 vs. P_2O_5 (C, after Li et al., 2007a) diagrams for the ore-related granitoids from the Xiaohekou skarn Cu deposit. The composition fields of intrusions associated with skarn Cu deposits worldwide are from Meinert (1995); composition data for Late Mesozoic granitoids associated with porphyry–skarn Cu mineralization in the Zha-Shan district are from Wu (2013), Meng et al. (2014), and Xie et al. (2015, 2017).

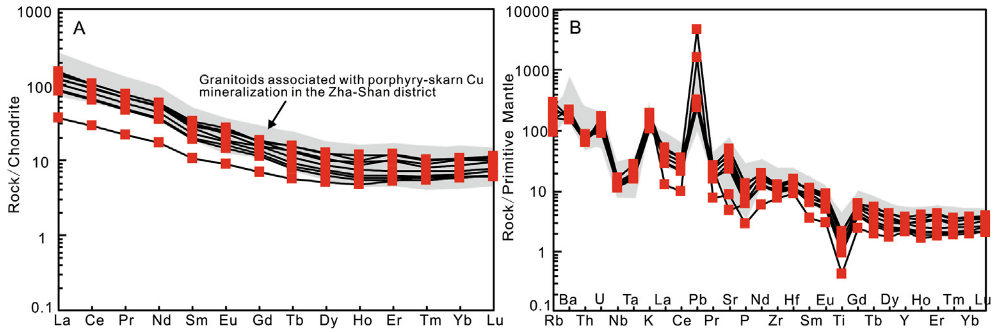

Fig. 9. (A) Chondrite-normalized REE patterns and (B) primitive mantle-normalized multi-element spider diagrams for the Xiaohekou ore-related granitoids.

weighted mean age of 141.3 ± 1.3 Ma (MSWD = 2.5), which can be interpreted as the crystallization age of granodiorite porphyry. Meanwhile, six analysis spots yield older $^{206}Pb/^{238}U$ ages of 492–922 Ma as inherited components. A total of 24 spots from sample XHX12 yield Th and U concentrations of 43.7–619 and 211–1838 ppm, respectively, with the Th/U ratios of 0.91–7.19, indicating a magmatic origin for the zircons (Hoskin, 2005). A total of 22 analysis spots yield a weighted U–Pb zircon age of 138.1 ± 2.0 Ma (MSWD = 2.3), which can be interpreted as the timing of crystallization for the granite porphyry. Two analysis spots have $^{206}Pb/^{238}U$ ages of 654 and 545 Ma, reflecting contamination by the Neoproterozoic basement rocks. Zircons with U–Pb ages of ~140 Ma from the Xiaohekou intrusions are prominently enriched in HREE relative to LREE, with positive Ce and negative Eu anomalies (Fig. 11), which are common features of magmatic zircons in igneous rocks (Hoskin, 2005). The Ti content in zircons from samples XH5 and XHX12 are 1.25–5.49 (average of 3.54 ppm) and 1.23–29.6 ppm (average of 4.75 ppm), respectively.

5.3. Magma oxygen fugacity estimated using Ce^{4+}/Ce^{3+} and ΔFMQ

Generally, Ce in zircons is a relatively sensitive and robust measure of the magmatic oxidation state due to multiple ionic states. Qualitative and quantitative estimates of fO_2 using zircon Ce^{4+}/Ce^{3+} ratios and ΔFMQ values are helpful in determining fO_2 in our study. The theories for calculating these ratios are proposed by Ballard (2002) and Trail et al. (2012). The Ce^{4+}/Ce^{3+} ratios are calculated on the basis of a lattice strain model (Blundy and Wood, 1994) for zircon–melt partitioning of Ce^{4+} and Ce^{3+} cations, assuming that the element

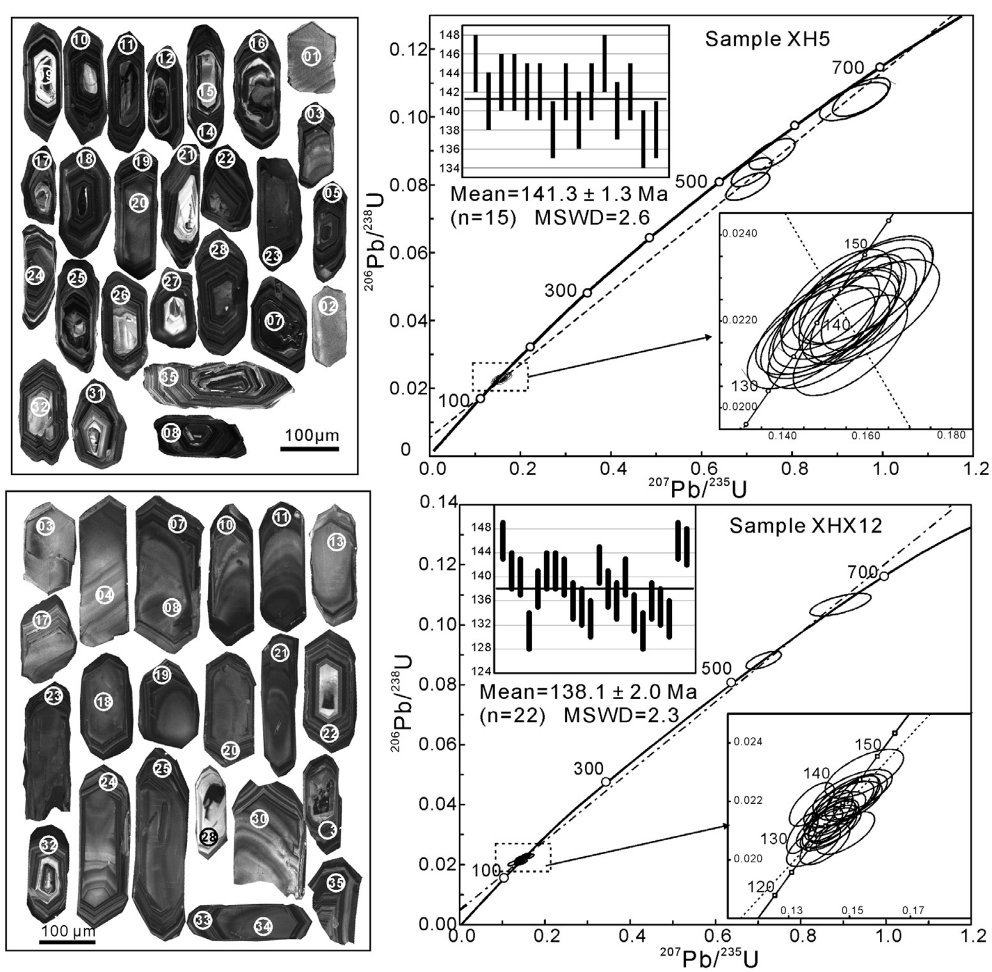

Fig. 10. Cathodoluminescence images and LA–ICP–MS zircon U–Pb concordia diagrams of ore-related granitoids.

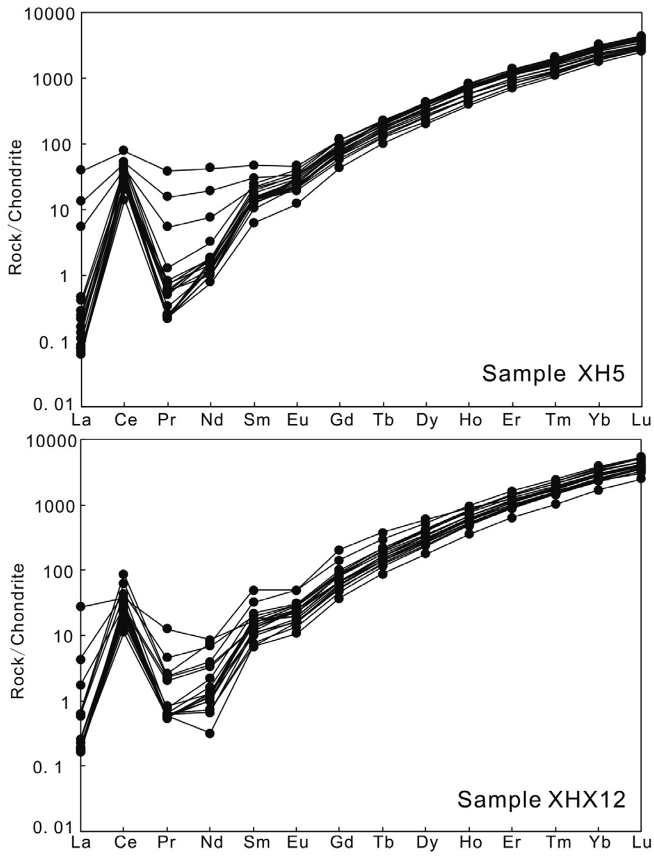

Fig. 11. Chondrite-normalized REE patterns of zircons for ore-related granitoids. Chondrite REE values are from Sun and McDonough (1989).

concentrations in the melt are equal to those in the bulk rock (Ballard et al., 2002). The Ti-in-zircon thermometer (Ferry and Watson, 2007) is employed to estimate zircon crystallization temperature (T_{zircon}) by setting the activities of SiO_2 and TiO_2 to 1 and 0.6, respectively (Qiu et al., 2013). δCe is computed with La–Pr interpolation. The introduction of a specific mineral oxidation buffer for fayalite–magnetite–quartz (FMQ buffer) yields the following expressions:

$$\text{FMQ buffer} = -24{,}441.9/(T + 273) + 8.290 \quad (\pm 0.167)$$

(600 °C − 1140 °C, Myers and Eugster, 1983)

$$\Delta\text{FMQ} = \lg fO_2 - \text{FMQ buffer}.$$

Zircons of samples XH5 and XHX12 have crystallization temperatures of 617–738 °C (average of 691 °C) and 616–922 °C (average of 695 °C), respectively. The calculated zircon ΔFMQ values for samples XH5 and XHX12 are −10.3 to +8.82 (average of +2.12) and −9.78 to +7.38 (average of +0.50). The Ce^{4+}/Ce^{3+} ratios are 33–736 (average of 419) and 101–882 (average of 484), respectively (Table ES3).

5.4. Zircon Lu–Hf isotopes

In situ Lu–Hf isotopic compositions of zircon grains are presented in Table ES4 and Fig. 12. A total of 12 zircons with the weighted mean age of 141 Ma from sample XH5 have $^{176}Hf/^{177}Hf$ ratios of 0.282602–0.282760, which computed the $\varepsilon_{Hf}(t)$ values from −3.06 to +2.45 (average of −0.62), with corresponding T_{DM2} values of 1.4–1.0 Ga (average of 1.2 Ga). A total of 15 zircons with a mean age of 138 Ma from sample XHX12 have $^{176}Hf/^{177}Hf$ ratios of 0.282550–0.282727 and yielded the $\varepsilon_{Hf}(t)$ values from −4.75 to +1.22 (average of −0.86), with corresponding T_{DM2} values of 1.5–1.1 Ga (average of 1.2 Ga).

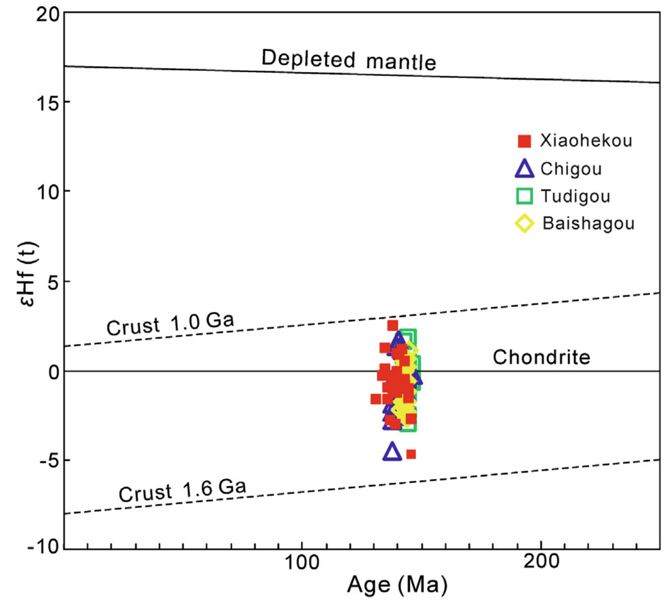

Fig. 12. Plot of zircon $\varepsilon_{Hf}(t)$ values vs. crystallization ages for the granitoids from the Xiaohekou Cu deposit.

6. Discussion

6.1. Petrogenesis of the ore-related granitoids in the Xiaohekou Cu deposit

The mineralization-related granitoids in the Xiaohekou mining district are characterized by relatively low SiO_2 (65.9–73.3 wt%) and MgO (0.26–1.72 wt%) contents with variable Mg# values (29.4–64.0), high K_2O (3.11–5.75 wt%) content and K_2O/Na_2O ratios (0.74–63.9, average of 6.08), and negligible Eu anomalies (δEu = 0.89–1.15), which indicate that slight plagioclase fractional crystallization occurred after the initial melt was formed. The samples also exhibit depletion in compatible elements, such as Cr (2.89–7.96 ppm), Ni (2.00–6.48 ppm), Nb (7.85–11.5 ppm), Ta (0.63–1.09 ppm), and Ti (539–2637 ppm), high Sr/Y (46.6–64.7) and La/Yb (17.0–25.0) ratios, and low Y (9.6–16.2 ppm) and Yb (0.95–1.75 ppm) contents (Table ES1). Rapp et al. (1991) proposed that the lower crustal source comprising eclogite- or garnet-bearing amphibolites at depths of > 40–50 km can generate such high Sr/Y and La/Yb magma. These features of the Xiaohekou granitoids are similar to those of high-K calc-alkaline adakite-like magma formed by partial melting of thickened lower crust from continental collision zones or intracontinental setting, such as porphyries in the Gangdese belt and the Middle–Lower Yangtze River Valley metallogenic belt in eastern China (Rapp et al., 1991; Hou et al., 2004, 2013; Hou and Yang, 2009; Chung et al., 2009; Pirajno and Zhou, 2015; Zhou et al., 2015; Xu et al., 2016). Geophysical investigations have illustrated that the thickness of the Qinling crust is > 50 km as a result of intracontinental subduction and double-vergent thrusting and thickening during the Late Jurassic to Early Cretaceous (Zhang et al., 2001; Dong and Santosh, 2016).

Most Xiaohekou granitoids are metaluminous to weakly peraluminous with low A/CNK values (average of 0.95) and have low Rb/Sr (0.07–0.22) and Rb/Ba (0.04–0.17) ratios, featuring a magmatic assemblage of 10% to 15% amphibole and biotite (Fig. 7) but lacking Al-rich minerals (e.g., muscovite, cordierite, and garnet), consistent with an I-type magma affinity (Chappell, 1999; Chappell and White, 2001). Moreover, the significant negative correlation between P_2O_5 and SiO_2 contents (Fig. 8C), i.e., typical of an I-type granite evolution trend, indicates that the magma could have been derived from partial melting of metaigneous rocks (Chappell and White, 2001; Li et al., 2007a). Given that mantle-derived materials contributed to the formation of I-type granite to varying degrees, zircons of the Xiaohekou granitoids

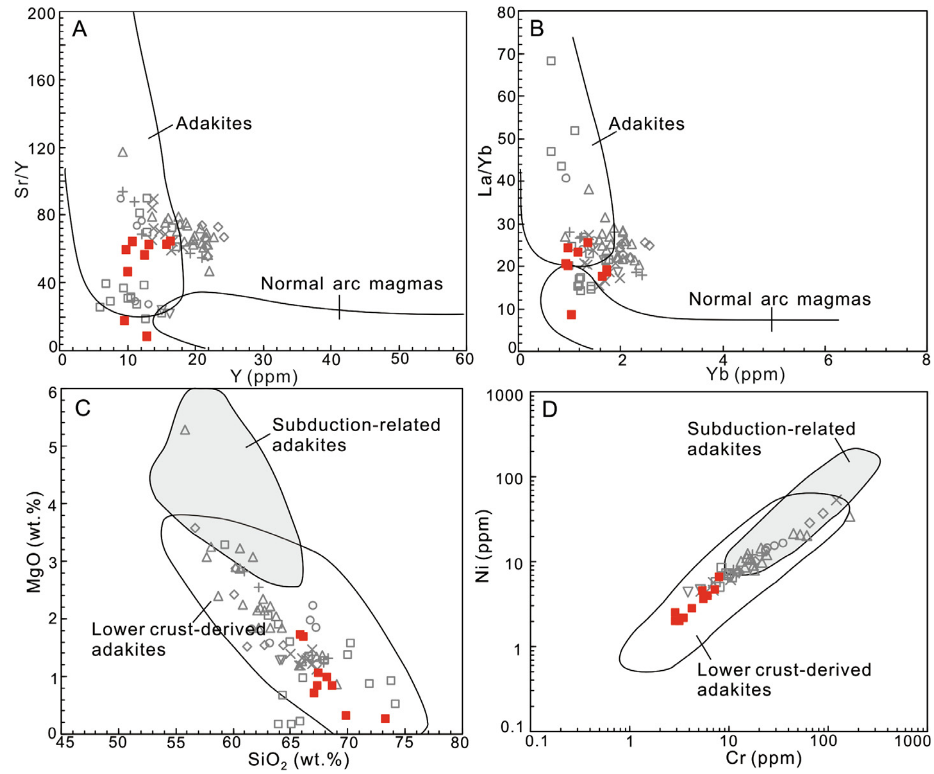

Fig. 13. Adakite geochemical discrimination diagrams of (A) Sr/Y vs. Y (after Defant and Drummond, 1990); (B) La/Yb vs. Yb (after Martin, 1999); C MgO vs. SiO_2 (after Zhou et al., 2015) and (D) Ni vs. Cr (after Guan et al., 2012) for the ore-related granitoids from the Xiaohekou Cu deposit. Symbols as in Fig. 8.

studied here have positive $\varepsilon_{Hf}(t)$ values (0 to +2.45), which indicate that there must have been an input of mantle-derived melt. Chen et al. (2014) obtained high $Mg/(Mg + Fe^{3+} + Fe^{2+})$ (> 0.5) and $Fe^{3+}/(Fe^{3+} + Fe^{2+})$ (> 0.1) ratios and low Al^{VI} values (average of 0.12) of biotite and $Mg/(Mg + Fe^{2+})$ (0.53–0.95) of amphibole from granitic stocks in the Zha-Shan ore cluster area and proposed that the data are consistent with the compositions of biotite and amphibole in I-type granitoids, which are sourced from hybrid (mantle + crust)-derived mafic and felsic magmas. In the $\varepsilon_{Hf}(t)$ vs. age diagram, the ore-related granitoids in the Xiaohekou mining district have variable $\varepsilon_{Hf}(t)$ values within a narrow range near the chondrite line (Fig. 12), meaning that pure lower crust materials could not be the only source region that generates magmas. These ore-related granitoids have T_{DM2} of 1.5–1.2 Ga (average of 1.28 Ga), corresponding to small negative $\varepsilon_{Hf}(t)$ values (–4.75 to –0.13), and T_{DM1} of 0.80–0.71 Ga (average of 0.76 Ga), corresponding to positive $\varepsilon_{Hf}(t)$ values (+0.07 to + 2.45). This finding further indicates that granodiorite porphyry and granite porphyry at Xiaohekou resulted from partial melting of Mesoproterozoic lower crustal rocks with additional contributions from Neoproterozoic mantle-derived magmas. In addition, more than one fourth of the $\varepsilon_{Hf}(t)$ values are positive, further indicating a significant contribution from the enriched lithospheric mantle for the Xiaohekou granitoids because zircons from depleted mantle have relatively high $\varepsilon_{Hf}(t)$ values. These granitoids also have consistent Hf isotopic compositions with the Chigou, Baishagou, and Lengshuigou granitoids ($\varepsilon_{Hf}(t)$ = –4.5 to +1.78), which are considered the mantle contributions that account for a large proportion of their formation (Wu et al., 2014; Ren et al., 2014; Xie et al., 2017). Similarly, this conclusion is compatible with the high (Mg + Ti)/Si and Mg + Ti values of magmatic biotite, as well as low I_{Sr} values (0.7045–0.7049) of apatite for the Late Mesozoic granitic stock at Xiaohekou, which was sourced from a combination of mantle-derived magma and various proportion of crustal components (Zhang et al., 1989). This is also supported by granites in the Chigou, Baishagou, and Lengshuigou deposits (or occurrences) with I_{Sr} values of 0.7046–0.7053 and isotopic composition $\varepsilon_{Nd}(t)$ values of −6.7 to −3.8, which are markedly different from the values of depleted mantle and lower crust (Xie et al., 2015, 2017).

In the SQO, a large number of outcrops of pre-Cambrian basement rocks are represented by the Douling Complexes and the Wudang and Yaolinghe Groups. The Douling Complex has a formation age of ~2.5 Ga and corresponding $\varepsilon_{Hf}(t)$ values of −4.5 to −1.2. Around t = 140 Ma, the calculated $\varepsilon_{Hf}(t)$ values are less than −20. The Wudang and Yaolinghe Groups were formed in the Neoproterozoic, as defined by detrital zircon U–Pb ages of 900–740 Ma (Ling et al., 2008; Wang et al., 2013b) and a whole-rock Sm–Nd isochron age of 1019 ± 81 Ma (Zhang et al., 1997). However, the granitoids in the Xiaohekou mining district have T_{DM2} values of 1.5–1.2 Ga, indicating that granitic magma was derived from partial melting of an unexposed Mesoproterozoic basement. Wu (2013) also reported zircon T_{DM2}(Hf) values of 1.39–1.22 Ga for the Xiaguanfang, 1.44–1.12 Ga for Yuanjiagou, 1.36–1.11 Ga for Chigou, and 1.44–1.11 Ga for Lengshuigou granitoids, which indicate that the Late Mesozoic granitoids in the Zha-Shan ore district have Mesoproterozoic sources. A previous study showed that significant crustal accretion occurred between 1.7 Ga and 1.0 Ga (peak at ~1.1 Ga) with considerable basic volcanic activity in the SQO (Zhang et al., 1997). Moreover, inherited zircons with U–Pb ages of 922, 654, 648, and 640 Ma obtained from this study (Table ES2) indicate that the initial magma of Xiaohekou granitoids capture overlying Neoproterozoic basement material during its emplacement. Hence, an unexposed Mesoproterozoic basement beneath the SQO is a potential contributor to the Late Mesozoic granitoids in the Zha-Shan ore district. As discussed above, we infer that the Xiaohekou granitoids were derived from partial melting of Mesoproterozoic rocks of the thickened lower crust, accompanied by interaction with the enriched lithospheric mantle-derived magma.

6.2. Magmatic oxygen fugacity and its implications for mineralization

A number of studies of porphyry–skarn Cu ± Mo deposits have demonstrated that magma compositions and oxygen fugacity conditions are two major factors influencing potential fertility (e.g., Hedenquist and Lowenstern, 1994; Ballard et al., 2002; Sun et al., 2013; Qiu et al., 2013; Yao et al., 2017; Cao et al., 2018). Crystallizing magmas with a characteristic I-type calc-alkaline signature would continuously concentrate volatiles dominated by magmatic-derived water. When volatility reaches saturation or oversaturation, melt–fluid immiscibility occurs in the volatile-rich silicate melt, fractionating a high temperature and high salinity magmatic–hydrothermal fluid with abundant volatiles and alkali. Such fluids have a strong capability to extract and carry metals, and supply the most important ore-forming components of hydrothermal fluids and metals to the skarn–porphyry mineralization system (Meinert, 1992, 1993; Hedenquist and Lowenstern, 1994; Davidson, 2001). In summary, the Xiaohekou ore-related granite porphyry and granodiorite porphyry belonging to high-K calc-alkaline I-type granitoids are derived from the thickened lower crust with an adakitic signature, and are accompanied by contemporaneous cryptoexplosion breccia in the ore district (Fig. 7A). These findings are consistent with the observation that most Cu and Fe deposits in the world are associated with I-type calc-alkaline porphyritic plutons, many of which have stockwork veins, brecciation, and intense hydrothermal alteration (Meinert, 1992, 1993; Hou et al., 2004; Hou and Yang, 2009; Pirajno, 2013; Xu et al., 2016; Goryachev et al., 2018). Moreover, such C-type adakitic rocks have significant potential for Cu mineralization because deep, high pressure, and high oxygen fugacity conditions are favorable for the pre-enrichment of abundant volatiles, Cu and sulfur in the source region (Hou and Yang, 2009; Zhang and Li, 2012). As shown in Figs. 8 and 14, the Xiaohekou ore-related granitoids share identical geochemical characteristics to the granitoids associated with skarn Cu deposits elsewhere in the world (Meinert, 1995). All these indicate that granitoids in the study area possess magma conditions favourable for forming Cu deposit.

A number of researchers have reported a persistent genetic link between oxidized magmas and processes leading to Cu ± Mo mineralization (Meinert, 1992; Richards et al., 2012; Ballard et al., 2002; Liang et al., 2006; Sun et al., 2013, 2015; Wang et al., 2013a; Qiu et al., 2013; Dilles et al., 2014; Wang et al., 2015c; Xu et al., 2016; Cao et al., 2018). This most probably involves redox control of the speciation and solubility of magmatic sulfur and its influence on the fractionation of chalcophile elements (Ballard et al., 2002). Metallogenic experiments show that Cu can be classified as a strong sulfophilic element and tends to distribute into magmatic sulfide phases (S^{2-}), rather than silicate melt or oxide minerals ($D_{\text{sulfide/silicate}}$ = 480–1303, Ripley et al., 2002). Thus, most Cu will be sequestered in sulfides trapped in cumulates in the early stages and will be unavailable to a late-stage magmatic–hydrothermal fluid (Ballard et al., 2002). However, Cu will be partitioned into the melt under higher fO_2 conditions during differentiation and transferred into a magmatic–hydrothermal fluid should the magma reach fluid saturation because, under oxidized conditions, magmatic sulfur exists mainly in the form of sulfate (SO_4^{2-}), which has a higher solubility in silicate melt than sulfide, and will suppress the formation of sulfide phases (S^{2-}) (Carroll and Rutherford, 1987; Ballard et al., 2002; Jugo et al., 2010; Richards et al., 2012; Sun et al., 2015). Moreover, a high oxidation state facilitates the decomposition of early residual sulfide phases in the magma source and activates Cu, Au, and PGE elements into the melt (Richards, 2003; Botcharnikov et al., 2011), thereby increasing Cu concentrations in evolved magma and favoring Cu mineralization. Zircons from the Xiaohekou granitoids have ΔFMQ values concentrating on −0.62 to +5.54, with the average of +1.34 (Table ES3). On the plots of lg(fO_2)–T vs. δCe–T (Fig. 14A, B), most samples from the Xiaohekou granitoids show the fO_2 of FMQ (Fe_2SiO_4–Fe_3O_4–SiO_2) to HM (Fe_2O_3–Fe_3O_4), and some samples reach the HM buffer. In addition, the values of lgfO_2 and δCe of the Xiaohekou granitoids are consistent with those of the Lannitang porphyry Cu deposit in the Sanjiang region in east Tibet and the Dongguashan skarn Cu deposit in the Tongling district in east China, suggesting a high oxidation state with the granitoids. These results agree with the popular occurrence of hydrothermal magnetite and hematite (martite or specularite) in the Xiaohekou skarn system (Fig. 6G, H, and P). The occurrence of magnetite and hematite generally represents the high fO_2 of the magmatic–hydrothermal Cu system because the oxidation of Fe^{2+} during the crystallization of magnetite and hematite is the causal process of SO_4^{2-} reduction and subsequent mineralization (Liang et al., 2009; Sun et al., 2013; Nadoll et al., 2015). Similarly, the Eu/Eu* value is another indicator of the oxidation state since the oxidation of Eu^{2+} in the melt can be induced by the reduction of magmatic SO_4^{2-} (Dilles et al., 2014), and zircon with Eu/Eu* > 0.4 is characteristic of many ore-forming magmas (Ballard et al., 2002). The Eu/Eu* values also show a positive correlation with the Ce^{4+}/Ce^{3+} ratios (Ballard et al., 2002). In comparison with the porphyries associated with large-giant Cu deposits in the Gangdese metallogenic belt (Tibet), Black Mountain (Philippines), and Chuquicamata-El Abra (northern Chile), the Xiaohekou ore-related granitoids investigated in this study exhibit similar or even higher Ce^{4+}/Ce^{3+} (average of 452) and Eu/Eu* (average of 0.72) values than these fertile deposits (Fig. 14C). The zircon 10,000(Eu/Eu*)/Y (> 1), (Ce/Nb)/Y (> 0.01), and Dy/Yb (< 0.3) ratios are also indicative of fertility (Lu et al., 2016), implying that the Xiaohekou granitoids might have the potential to produce a large magmatic–hydrothermal Cu deposit. In addition, the Xiaohekou rocks (up to 143 ppm) have higher Cu concentration than that of granitoids in the SQO (~11 ppm) (Zhang et al., 1994), indicating an anomalously Cu-rich magmatic system.

According to Meinert (1992, 1995), the magma sources of intrusions

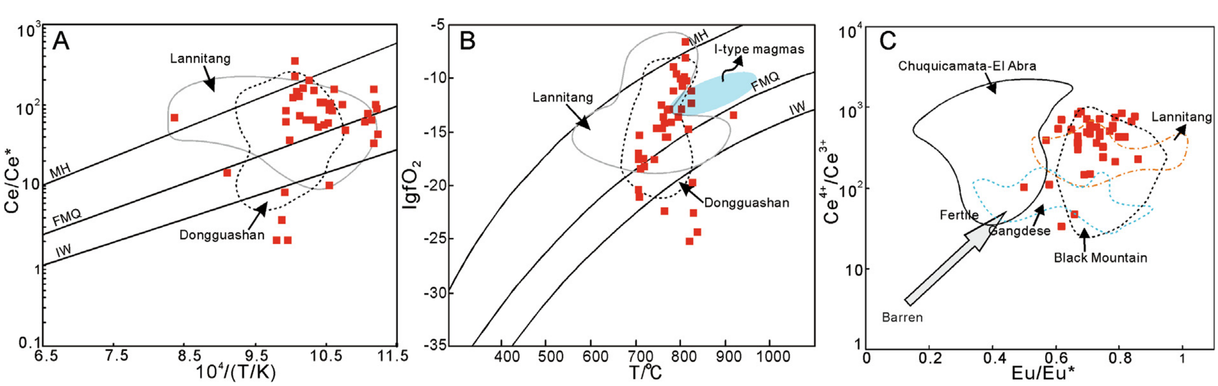

Fig. 14. Magma oxidation state of the Xiaohekou Cu deposit. (A) Ce/Ce* vs. 10^4/T; (B) lg(fO_2) vs. T; (C) Ce^{4+}/Ce^{3+} vs. Eu/Eu*. Data of the skarn Cu deposit of Dongguashan (eastern China) are from Wang et al. (2015c); Data of porphyry Cu deposits of Lanninan (Yunnan), Gangdese (Tibet), Black Mountain (Philippines) and Chuquicamata-EI Abra (northern Chile) are from Yu et al. (2016), Cao et al. (2018), Ballard et al. (2002).

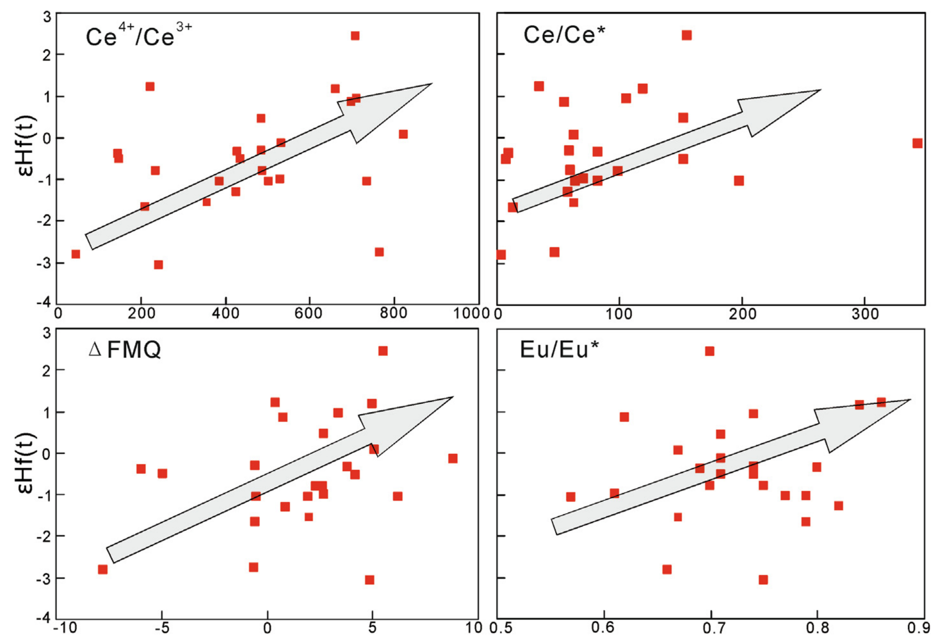

Fig. 15. Plots of $\varepsilon_{Hf}(t)$ vs. zircon Ce^{4+}/Ce^{3+}, Ce/Ce*, ΔFMQ, and Eu/Eu*.

associated with Fe, Au, and Cu skarn deposits usually have mantle materials involved. Many researchers have realized that the presence of a mantle component is one of the most critical factors for forming porphyries and associated ore deposits, not only by providing large amounts of metals and volatiles but also by optimizing the fO_2 condition (Meinert, 1993, 1995; Keith et al., 1997; Hattori and Keith, 2001; Maughan et al., 2002; Hou and Yang, 2009; Hou et al., 2013; Zhou et al., 2015; Xiong et al., 2016; Cao et al., 2018). The fO_2 response observed in this study also supports this interpretation. Our analysis of zircon Hf isotope compositions shows that the magma source of the Xiaohekou ore-related granitoids comprises more than one fourth of the enriched lithospheric mantle components. Indeed, these granitoids exhibit obvious elevation in zircon Ce^{4+}/Ce^{3+} ratios, ΔFMQ values, as well as Ce and Eu anomalies with increasing $\varepsilon_{Hf}(t)$ values (Fig. 15). This indicates that the involvement of the oxidized mantle components is the most likely factor to improve the magma fO_2, which might have played a key role in the formation of the Xiaohekou skarn Cu deposits. Thus, we argue that the Xiaohekou fertile magma associated with the skarn Cu deposit can be most probably produced by the mixing magma generated from the enriched lithospheric mantle and partial melting of the thickened lower continental crust. Mafic magma ascending from the mantle through the thickened lower crust became mixed up and homogenized with felsic magma. High fO_2 melts and/or fluids were supplied from the mafic magma into the mingling magma to form the fertile Cu-bearing magma. In addition, we propose that the granitic rocks with zircon $Ce^{4+}/Ce^{3+} > 452$, $\delta Eu > 0.72$, and $\Delta FMQ > +1.34$ can be helpful indicators for future exploration targets of the magmatic–hydrothermal deposits formed in the Zha-Shan ore district.

6.3. Timing and tectonic setting of magmatism and mineralization

Numerous small granitic intrusions, which control the distribution of porphyry–skarn deposits (or occurrences), extensively occur throughout the Zha-Shan ore district. However, in the past decade, limited radiometric ages for porphyry–skarn Cu and Mo deposits in this area have been documented. Thus, the tectono-chronological framework for the mineralization and associated intrusions has not been well established.

Zircon U–Pb dating of the mineralization-related granodiorite porphyry and granite porphyry in the study area have shown consistent emplacement ages of 141.3 ± 1.3 Ma and 138.1 ± 2.0 Ma within error. The new U–Pb ages (141–138 Ma) are similar to the zircon U–Pb ages (148–142 Ma) and molybdenite Re–Os isochron (or model) ages (151–146 Ma) obtained from the Chigou and Lengshuigou porphyry Cu–Mo deposits (Fig. 2; Li et al., 2011; Ren et al., 2014; Wu et al., 2014; Xie et al., 2015, 2017). Precise zircon U–Pb chronology in the Zha-Shan ore cluster shows that other granitoid intrusions at Shuangyuangou, Yuanzijie, Xiaguanfang, Tudigou, and Baishagou mineralized localities (Fig. 2) formed within a narrow time range of 148–138 Ma (Wu, 2013; Xie et al., 2015, 2017). The Xiaohekou granitoids and those contemporaneous granitoids with ages of 148–138 Ma share some remarkable geochemical signatures (Figs. 8, 9, and 13), such as low SiO_2 and MgO contents, high K_2O content, high Sr/Y and La/Yb ratios, negligible Eu anomalies, and pronounced Nb, Ta, Ti, Cr and Ni negative anomalies. Thus, the age data and geochemical features indicate that these granitoids were probably generated from a single tectono–magmatic event and attest to the fact that magmatism and metallogenesis in the Zha-Shan district overlapped in terms of time.

The Late Jurassic–Early Cretaceous granitoids and associated 151–138 Ma porphyry–skarn Cu and Mo deposits in the Zha-Shan district share an almost identical age range with a large number of granitoids aged at 158–130 Ma in the NQO and S-NCB between 109 °E and 112 °E (Li et al., 2018 and references therein). The tectonic setting accounting for the Late Mesozoic magmatism and metallogenesis is still controversial. At least four alternative models have been proposed: (1) syn-collision (Li et al., 2007, 2012c; Yang et al., 2012) or (2) post-collision evolution following the continental collision between the SCB and NCB (Chen et al., 2004, 2009; Chen, 2010; Bao et al., 2014; Yang et al., 2015; Zhou et al., 2016; Li et al., 2015, 2018). (3) Paleo-Pacific slab subducting northwestward beneath the East China (Mao et al., 2008, 2011; Li et al., 2012a, 2019; Pirajno and Zhou, 2015); (4) Intracontinental orogeny, suggesting that after the culmination of continental collision orogenesis in T_{2-3}, the entire Qinling Orogen evolved into an intracontinental orogenic evolution process (Zhang et al., 1995, 2001; Wang et al., 2011a; Li et al., 2012b; Heberer et al., 2014; Dong et al., 2016; Dong and Santosh, 2016). We prefer to relate the Late Jurassic–Early Cretaceous granitoids in the Zha-Shan district to the intracontinental orogeny, on the basis that the renewed southward intracontinental subduction of the NCB and the continuous northward subduction of the SCB, beneath the Qinling Orogen, led to the dramatic

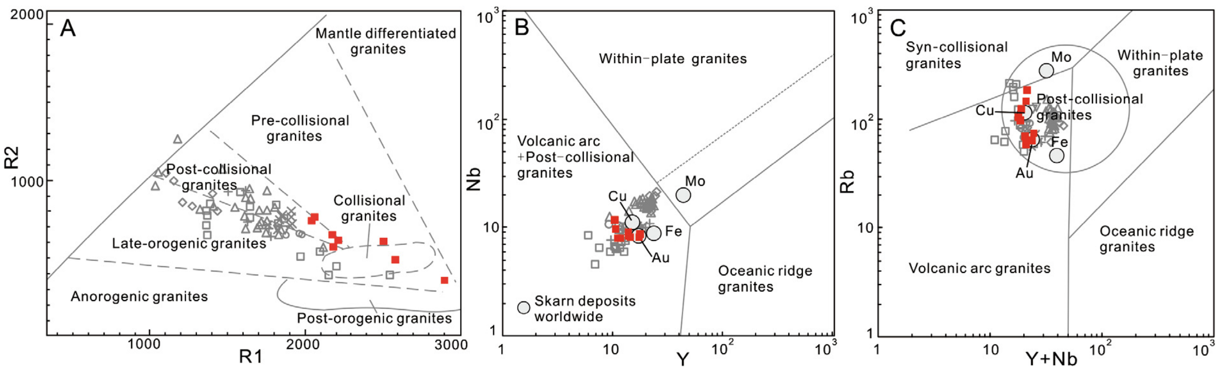

Fig. 16. Tectonic discrimination diagrams of (A) R1 vs. R2 (after Batchelor and Bowden, 1985); (B) Nb vs. Y, and (C) Rb vs. Y + Nb (after Pearce et al., 1984). Symbols as in Fig. 8.

N–S compression and thrust–nappe structures as well as mountain uplift and denudation in the entire Qinling Orogen revealed by the geophysical investigations (Yuan, 1996; Zhang et al., 1995, 2001; Dong and Santosh, 2016). The extensive intracontinental tectono-magmatism and Au–Mo metallogenesis in the Qinling Orogen formed within this geodynamic context (Dong and Santosh, 2016).

The adakitic geochemical signature of the Xiaohekou granitoids shown by this study can be interpreted as evidence that the materials originated from the thickened lower crust, with the thickening caused by the intense intracontinental subduction in the Late Jurassic mentioned previously. This model is consistent with that proposed by Zhou et al. (2015), who argued that the Jurassic–Cretaceous porphyry–skarn Cu–An mineralization in the Middle–Lower Yangtze River Metallogenic Belt in east China, with most porphyries exhibiting adakitic affinity, occurred in the typical intracontinental environment. As proposed by Hou and Yang (2009), in an intracontinental environment, ore-forming magmas are derived from partial melting of a delaminated lithosphere root. In the R1–R2, and Y–Nb and Y + Nb–Rb diagrams (Fig. 16), all of the granitoid samples plot into the post-collisional (uplift) granite fields, indicating that the Xiaohekou granitoids exhibit post-collisional magma affinity and seem to be induced by an intracontinental orogeny after the peak of N–S compression. Previous studies have already shown that the later period of major orogenic episodes is usually marked by strong uplift and erosion, large movements along transcurrent shear zones and extensional tectonic regimes induced partly by both the gravitational collapse of thickened crust and the delamination of the lithosphere. Moreover, the post-collisional association is characterized by abundant high-K calc-alkaline to alkaline igneous suites, enrichment in LILE and LREE, and depletion in HFSE, as well as markedly rich alkali, Sr, and Ba relative to island arc igneous rocks (Liégeois, 1998; Bonin, 2004). These geochemical characteristics are observed for the Xiaohekou granitoids, reflecting that they are probably post-collisional granitoids emplaced in an extensional regime. From the perspective of geochemistry and geochronology, our results are compatible with the post-collisional model. However, considering the intense intracontinental orogeny and that the SQO had witnessed a post-collisional process during ca. 212–200 Ma, which is represented by the lamprophyre and Shahewan, Qinlingliang and Laojunshan intrusions with rapakivi-texture, and transitional geochemical compositions from I to A-type granite (Lu et al., 1999; Wang et al., 2007, 2011b; Zhang et al., 2008), we here propose that the "post-collisional" signature for the Xiaohekou granitoids means postdating the intracontinental orogeny, rather than continental collision between the SCB and NCB.

Crustal and lithospheric thinning is clearly recorded in the Eastern Qinling Orogen, with 150–157 Ma delamination (Li et al., 2012b), e.g., the Muhuguan pluton (~ 150 Ma) located to the north of the Xiaohekou granitoids contains microgranular mafic enclaves (Liu et al., 2013) and ~ 148 Ma mafic dykes reported in the Luanchuan Mo district in the S-NCB (Bao et al., 2014). These are considered to involve mantle-derived components during the Late Jurassic Qinling intracontinental orogeny. As mentioned above, the Shanyang fault–bounded basin where the Zha-Shan ore district is located is thought to have formed in an extensional collapse regime during the Cretaceous (Dong and Santosh, 2016). Moreover, in the field, a number of NE–NNE-trending strike–slip faults are observed crosscutting the EW-trending faults to form the intersections where the ore-forming granitoids intruded (Fig. 2) (Yan et al., 2014). These faults could be comparable with the developed NNE-trending faults generated by extension within the S-NCB (Chen and Fu, 1992; Zhai et al., 2004; Li et al., 2012a), reflecting that the SQO stress field also gradually transformed to extensional in nature during the Early Cretaceous. Similarly, based on a comprehensive compilation of Late Mesozoic granitoids in the Qinling Orogen, Li et al. (2018) recently proposed that the Late Mesozoic tectonic regime of the Qinling Orogen was a synthesis effect of post-collisional transition from compression to extension, and back-arc extension related to Paleo-Pacific subduction. Numerous studies suggested that the Early Cretaceous magmatism–metallogenesis in the S-NCB and east China were related to the transformation of the tectonic–dynamic system from pre-Mesozoic Tethyan tectonics to Late Mesozoic Pacific tectonics, corresponding to the stress field transition from N–S to E–W-trending (Zhang et al., 2001; Lu et al., 2002; Li et al., 2007b, 2015; Mao et al., 2008, 2011; Zhu et al., 2010; Li et al., 2012b,c; Zhou et al., 2015) and the transition from intracontinental subduction thickening to large-scale lithospheric delamination and thinning (Mao et al., 2008, 2011). In addition, far-field effect from the plate boundary can be more effectively applied to intracontinental deformation (Li et al., 2019). Thus, we inferred that the ore-related granitoids in the Xiaohekou mining district were formed in the post-collisional compression–extension transition regime during the Early Cretaceous Qinling intracontinental orogeny (Fig. 17). This orogeny and subsequent extensional regime and large-scale lithospheric delamination were possibly induced by far-field effect of plate tectonics based on low-angle subduction of the Paleo-Pacific Plate (Li and Li, 2007). Given the lithospheric collapse and delamination beneath the Qinling Orogen, upwelling of the asthenospheric mantle supplied sufficient heat to develop partial melting of remanent enriched lithospheric mantle. The mafic magmas rising through the thickened lower continental crust led to partial melting and generated hybrid (crust + mantle)-derived fertile magmas with adakitic signature (Fig. 17).

7. Conclusions

(1) The Xiaohekou Cu deposit is a typical skarn-type Cu deposit. Orebodies are mainly developed in the skarn and marble in exocontact zones of granitoids. Four mineralization stages of the deposit are identified as follows: an anhydrous skarn stage, a hydrous skarn–oxide stage, a quartz–polymetallic sulfide stage, and a carbonate–quartz stage.

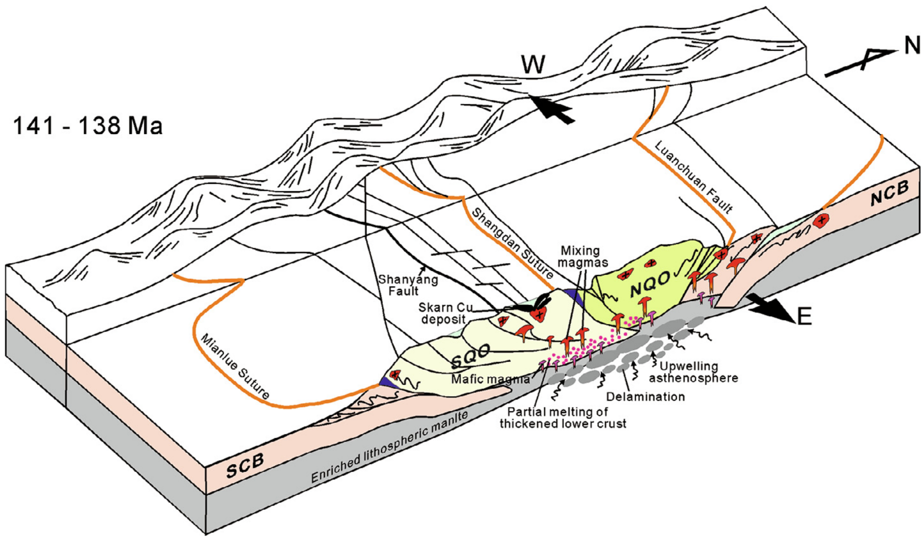

Fig. 17. Genetic model for the Early Cretaceous tectonic setting and formation of associated granitoids in the Zha-Shan ore district.

(2) The ore-forming granitoids were most likely produced by the mixing of magmas generated from the delamination of enriched lithospheric mantle and partial melting of the thickened mafic lower crust. During mixing and homogenization, high fO_2 melts or fluids were supplied from the mafic magmas into the mingling magmas to form the fertile Cu-bearing magma.

(3) The Xiaohekou granitoids have both the magma compositions and fO_2 conditions suitable for forming a large magmatic–hydrothermal Cu deposit. Granitic rocks with zircon $Ce^{4+}/Ce^{3+} > 452$, $\delta Eu > 0.72$, and $\Delta FMQ > +1.34$ can be encouraging indicators for future exploration targeting of the magmatic–hydrothermal deposits formed in the Zha-Shan ore district.

(4) The ore-related granitoids in the Xiaohekou mining district have consistent emplacement ages of 141.3 ± 1.3 Ma to 138.1 ± 2.0 Ma. These granitoids were formed in a post-collisional, compression to extension transitional regime during the Qinling intracontinental orogeny in the early Cretaceous. The transition was related to the transformation of the tectonic–dynamic system from pre-Mesozoic Tethyan tectonics to Late Mesozoic Pacific tectonics, corresponding to a change from a N–S to E–W trending stress field and from intracontinental subduction thickening to large-scale lithospheric delamination and thinning.

Acknowledgments

This study was jointly supported by National Natural Science Foundation of China (Grant Nos. 41730426, 41803039, 41421002 and 41272092), China Postdoctoral Science Foundation (Grant no. 2018M643712), and MOST Special Fund from the State Key Laboratory of Continental Dynamics, Northwest University, China. We sincerely thank Prof. Yanjing Chen and two anonymous reviewers for their constructive comments. Thanks are also given to Kai Liu and Yanhui Guo for the help during fieldwork, Prof. Simon Williams for English polishing, and Jianqi Wang, Ye Liu, and Huadong Gong for their assistance during the analyses.

References

Ames, L., Zhou, G.Z., Xiong, B.C., 1996. Geochronology and isotopic character of ultrahighpressure metamorphism with implications for collision of the Sino-Korean and Yangtze cratons, central China. Tectonics 15, 472–489.

Ballard, J.R., Palin, M.J., Campbell, I.H., 2002. Relative oxidation states of magmas inferred from Ce(IV)/Ce(III) in zircon: application to porphyry copper deposits of northern Chile. Contrib. Mineral. Petrol. 144, 347–364.

Bao, Z.W., Wang, C.Y., Zhao, T.P., Li, C.J., Gao, X.Y., 2014. Petrogenesis of the Mesozoic granites and Mo mineralization of the Luanchuan ore field in the East Qinling Mo mineralization belt, Central China. Ore Geol. Rev. 57, 132–153.

Batchelor, R.B., Bowden, P., 1985. Petrogenetic interpretation of granitoid rock series using multicationic parameters. Chem. Geol. 48, 43–55.

Blundy, J., Wood, B., 1994. Prediction of crystal melt partition coefficients from elasticmoduli. Nature 35 (6), 1126–1157.

Bonin, B., 2004. Do coeval mafic and felsic magmas in post-collisional to within-plate regimes necessarily imply two contrasting, mantle and crustal, sources? A review. Lithos 78, 1–24.

Botcharnikov, R.E., Linnen, R.L., Wilke, M., Holtz, F., Jugo, P.J., Berndt, J., 2011. High gold concentrations in sulphide-bearing magma under oxidizing conditions. Nature Geosci. 4, 112–115.

Bouvier, A., Vervoort, J.D., Patchett, P.J., 2008. The Lu–Hf and Sm–Nd isotopic composition of CHUR: constraints from unequilibrated chondrites and implications for the bulk composition of terrestrial planets. Earth Planet. Sci. Lett. 273 (1–2), 48–57.

Cao, M.J., Qin, K.Z., Li, G.M., Evans, N.J., McInnes, B.I.A., Li, J.X., Zhao, J.X., 2018. Oxidation state inherited from the magma source and implications for mineralization: late Jurassic to Early Cretaceous granitoids, Central Lhasa subterrane, Tibet. Miner. Deposita 53, 299–309.

Carroll, M.R., Rutherford, M.J., 1987. The stability of igneous anhydrite: experimental results and implications for sulfur behavior in the 1982 El Chichon trachyandesiteand other evolved magmas. J. Petrol. 28, 781–801.

Chappell, B.W., 1999. Aluminium saturation in I- and S-type granites and the characterization of fractionated haplogranites. Lithos 46, 535–551.

Chappell, B.W., White, A.J.R., 2001. Two contrasting granite types: 25 years later. Aust. J. Earth Sci. 48, 489–499.

Chen, Y.J., 2010. Indosinian tectonic setting, magmatism and metallogenesis in Qinling Orogen, central China. Geol. China 37, 854–865 (in Chinese with English abstract).

Chen, Y.J., Fu, S.G., 1992. Gold Mineralization in West Henan. China Seismological Press, Beijing pp. 234–250 (in Chinese with English abstract).

Chen, Y.J., Li, C., Zhang, J., Li, Z., Wang, H.H., 2000. Sr and O isotopic characteristics of porphyries in the Qinling molybdenum deposit belt and their implication to genetic mechanism and type. Sci. China Ser. D Earth Sci. 43, 82–94.

Chen, Y.J., Pirajno, F., Sui, Y.H., 2004. Isotope geochemistry of the Tieluping silver deposit, Henan, China: a case study of orogenic silver deposits and related tectonic setting. Miner. Deposita 39, 560–575.

Chen, Y.J., Pirajno, F., Li, N., Guo, D.S., Lai, Y., 2009. Isotope systematics and fluid inclusion studies of the Qiyugou breccia pipe-hosted gold deposit, Qinling Orogen, Henan province, China: implications for ore genesis. Ore Geol. Rev. 35, 245–261.

Chen, L., Yan, Z., Wang, Z.Q., Wu, F.F., Wang, R.T., Ren, T., Guo, Y.H., Wang, P., 2014. Mineralogical characteristic of the Yanshanian granitic rocks in Shanyang-Zhashui ore concentration area: an indicator for the magmatic nature and metallogenesis. Acta Geol. Sin. 88, 109–133 (in Chinese with English abstract).

Chung, S.L., Chu, M.F., Ji, J.Q., O'Reilly, S.Y., Pearson, N.J., Liu, D.Y., Lee, T.Y., Lo, C.H., 2009. The nature and timing of crustal thickening in Southern Tibet: geochemical and zircon Hf isotopic constraints from post-collisional adakites. Tectonophysics 477, 36–48.

Davidson, P., 2001. Immiscibility and continuous felsic melt-fluid evolution within the Rio Blanco porphyry system, Chile: evidence from inclusions in magmatic quartz. Econ. Geol. 96, 1921–1929.

Defant, M.J., Drummond, M.S., 1990. Derivation of some modern arc magmas by melting of young subducted lithosphere. Nature 347 (6294), 662–665.

Deng, X.H., Chen, Y.J., Pirajno, F., Li, N., Yao, J.M., Sun, Y.L., 2017. The geology and geochronology of the Waifangshan Mo-quartz vein cluster in eastern Qinling, China. Ore Geol. Rev. 81, 548–564.

Dilles, J.H., Kent, A.J.R., Wooden, J.L., Tosdal, R.M., Koleszar, A., Lee, R.G., Farmer, L.P., 2014. Zircon compositional evidence for sulfur-degassing from ore-forming arc

magmas. Econo. Geol. 110, 241–251.
Dong, Y.P., Santosh, M., 2016. Tectonic architecture and multiple orogeny of the Qinling Orogenic Belt, Central China. Gondwana Res. 29, 1–40.
Dong, Y.P., Yang, Z., Liu, X.M., Sun, S.S., Li, W., Cheng, B., Zhang, F.F., Zhang, X.N., He, D.F., Zhang, G.W., 2016. Mesozoic intracontinental orogeny in the Qinling Mountains, central China. Gondwana Res. 30, 144–158.
Ferry, J.M., Watson, E.B., 2007. New thermodynamic models and revised calibrations for the Ti-in-zircon and Zr-in-rutile thermometers. Contrib. Mineral. Petrol. 154, 429–437.
Goryachev, N.A., Shpikerman, V.I., Church, S.E., Gvozdev, V.I., 2018. Calcic skarn ore deposits of the North-East Russia. Ore Geol. Rev. 103, 3–20.
Guan, Q., Zhu, D.C., Zhao, Z.D., Dong, G.C., Zhang, L.L., Li, X.W., Liu, M., 2012. Crustal thickening prior to 38 Ma in southern Tibet: evidence from lower crust-derived adakitic magmatism in the Gangdese Batholith. Gondwana Res. 2, 88–99.
Guo, B., Yan, C.H., Zhang, S.T., Han, J.W., Yun, H., Tan, H.Y., Song, Q.C., Meng, F.X., 2018. Geochemical and geological characteristics of the granitic batholith and Yuku concealed Mo-W deposit at the southern margin of the North China Craton. Geol. J. https://doi.org/10.1002/gj.3372.
Hattori, K., Keith, J.D., 2001. Contribution of mafic melt to porphyry copper mineralization: evidence from Mount Pinatubo, Philippines, and Bingham Canyon, Utah, USA. Miner. Deposita 36, 799–806.
Heberer, B., Anzenbacher, T., Neubauer, F., Genser, J., Dong, Y.P., Dunkl, I., 2014. Polyphase exhumation in the western Qinling Mountains, China: Rapid Early Cretaceous cooling along a lithospheric-scale tear fault and pulsed Cenozoic uplift. Tectonophysics 617, 31–43.
Hedenquist, J.W., Lowenstern, J.B., 1994. The role of magmas in the formation of hydrothermal ore deposits. Nature 370, 519–527.
Hoskin, P.W.O., 2005. Trace-element composition of hydrothermal zircon and the alteration of Hadean zircon from the Jack Hills, Australia. Geochim. Cosmochim. Acta 69, 637–648.
Hou, Z.Q., Yang, Z.M., 2009. Porphyry deposits in continental settings of China: geological characteristics, magmatic-hydrothermal system, and metallogenic model. Acta Geol. Sin. 83, 1779–1817 (in Chinese with English abstract).
Hou, Z.Q., Gao, Y.F., Qu, X.M., Rui, Z.Y., Mo, X.X., 2004. Origin of adakitic intrusives generated during mid-Miocene east–west extension in southern Tibet. Earth Planet Sci. Lett. 220, 139–155.
Hou, Z.Q., Zheng, Y.C., Yang, Z.M., Rui, Z.Y., Zhao, Z.D., Jiang, S.H., Qu, X.M., Sun, Q.Z., 2013. Contribution of mantle components within juvenile lower-crust to collisional zone porphyry Cu systems in Tibet. Miner. Deposita 48, 173–192.
Hu, F.Y., Liu, S.W., Santosh, M., Deng, Z.B., Wang, W., Zhang, W.Y., Yan, M., 2016. Chronology and tectonic implications of Neoproterozoic blocks in the South Qinling Orogenic Belt, Central China. Gondwana Res. 30, 24–47.
Jackson, S.E., Pearson, N.J., Griffin, W.L., Belousova, W.A., 2004. The application of laser ablation-inductively coupled plasma-mass spectrometry to in situ U-Pb zircon geochronology. Chem. Geol. 211, 47–69.
Jugo, P.J., Wilke, M., Botcharnikov, R.E., 2010. Sulfur K-edge XANES analysis of natural and synthetic basaltic glasses: Implications for S speciation and S content as function of oxygen fugacity. Geochim. Cosmochim. Acta 74, 5926–5938.
Keith, J.D., Whitney, J.A., Hattori, K., Ballantyne, G.H., Christiansen, E.H., Barr, D.L., Cannan, T.M., Hook, C.J., 1997. The role of magmatic sulfides and mafic alkaline magmas in the Bingham and Tintic Mining Districts, Utah. J. Petrol. 38, 1679–1698.
Li, Z.X., Li, X.H., 2007. Formation of the 1300-km-wide intracontinental orogen and postorogenic magmatic province in Mesozoic South China: a flat-slab subduction model. Geology 35, 179–182.
Li, X.H., Li, W.X., Li, Z.H., 2007a. On the genetic classification and tectonic implications of the Early Yan shanian granitoids in the Nanling Range, South China. Chin. Sci. Bull. 52, 873–1885.
Li, N., Chen, Y.J., Zhang, H., Zhao, T.P., Deng, X.H., Wang, Y., Ni, Z.Y., 2007b. Molybdenum deposits in East Qinling. Earth Sci. Front. 14, 186–198 (in Chinese with English abstract).
Li, Q.G., Liu, S.W., Wang, Z.Q., Wang, D.S., Yan, Z., Yang, K., Wu, F.H., 2011. Late Jurassic Cu-Mo mineralization at the Zhashui-Shanyang district, South Qinling, China: constraints from Re-Os molybdenite and laser ablation-inductively coupled plasma mass spectrometry U-Pb zircon dating. Acta Geol. Sin. 85, 661–672.
Li, C.Y., Wang, F.Y., Hao, X.L., Ding, X., Zhang, H., Ling, M.X., Zhou, J.B., Li, Y.L., Fan, W.M., Sun, W.D., 2012a. Formation of the world's largest molydbenum metallogenic belt: a plate-tectonic perspective on the Qinling molybdenum deposit. Int. Geol. Rev. 54, 1093–1112.
Li, D., Zhang, S.T., Yan, C.H., Wang, G.W., Song, Y.W., Ma, Z.B., Han, J.W., 2012b. Late Mesozoic time constraints on tectonic changes of the Luanchuan Mo belt, East Qinling orogen, Central China. J. Geodyn. 61, 94–104.
Li, N., Ulrich, T., Chen, Y.J., Thompson, T.B., Peace, V., Pirajno, F., 2012c. Fluid evolution of the Yuchiling porphyry Mo deposit, East Qinling, China. Ore Geol. Rev. 48, 442–459.
Li, N., Chen, Y.J., Santosh, M., Pirajno, F., 2015. Compositional polarity of Triassic granitoids in the Qinling Orogen, China: implication for termination of the northernmost paleo-Tethys. Gondwana Res. 27, 244–257.
Li, N., Chen, Y.J., Santosh, M., Pirajno, F., 2018. Late Mesozoic granitoids in the Qinling Orogen, Central China, and tectonic significance. Earth Sci. Rev. 182, 141–173.
Li, S.Z., Suo, Y.H., Li, X.Y., Zhou, J., Santosh, M., Wang, P.C., Wang, G.Z., Guo, L.L., Yu, S.Y., Lan, H.Y., Dai, L.M., Zhou, Z.Z., Cao, X.Z., Zhu, J.J., Liu, B., Jiang, S.H., Wang, G., Zhang, G.W., 2019. Mesozoic tectono-magmatic response in the East Asian ocean-continent connection zone to subduction of the Paleo-Pacific Plate. Earth Sci. Rev. 192, 91–137.
Liang, H.Y., Campbell, I.H., Allen, C., Sun, W.D., Liu, C.Q., Yu, H.X., Xie, Y.W., Zhang, Y.Q., 2006. Zircon Ce^{4+}/Ce^{3+} ratios and ages for Yulong ore-bearing porphyries in eastern Tibet. Miner. Deposita 41, 152–159.
Liang, H.Y., Sun, W.D., Su, W.C., Zartman, R.E., 2009. Porphyry copper–gold mineralization at Yulong, China, promoted by decreasing redox potential during magnetite alteration. Econ. Geol. 104, 587–596.
Liégeois, J.P., 1998. Preface–some words on the post-collisional magmatism. Lithos 45, 5–17.
Ling, W.L., Ren, B.F., Duan, R.C., Liu, X.M., Mao, X.W., Peng, L.H., Liu, Z.X., Cheng, J.P., Yang, H.M., 2008. Timing of the Wudangshan, Yaolinghe volcanic sequences and mafic sills in South Qinling: U-Pb zircon geochronology and tectonic implication. Chin. Sci. Bull. 53, 2192–2199.
Liu, R., Li, J.W., Bi, S.J., Hu, H., Chen, M., 2013. Magma mixing revealed from in situ zircon U-Pb-Hf isotope analysis of the Muhuguan granitoid pluton, eastern Qinling Orogen, China: implications for late Mesozoic tectonic evolution. Int. J. Earth Sci. 102, 1583–1602.
Liu, K., Ren, T., Meng, D.M., Li, J.B., Wang, X.Y., Guo, Y.H., Yang, Z.H., 2014. Metallogenic regularities of porphyry copper deposits and prospecting direction in the Zhashui-Shanyang ore concentration area, Qin Ling orogenic belt. Geol. Exploartion 50 (6), 1096–1108 (in Chinese with English abstract).
Liu, K., Ren, T., Cao, G.J., Zhang, X.S., Yin, Y., Zheng, Z.L., Dang, K.F., Liu, Z.M., 2015. Geological characteristics and prospecting potential of the Mujiazhuang copper deposit, Shaanxi. Mineral Exploration 6 (2), 122–131 (in Chinese with English abstract).
Lu, X.X., Wei, X.D., Xiao, Q.H., Zhang, Z.Q., Li, H.M., Wang, W., 1999. Geochronological studies of rapakivi granites in Qinling and its geological implications. Geol. J. China Univ. 5, 372–377 (in Chinese with English abstract).
Lu, X.X., Yu, Z.P., Feng, Y.L., Wang, Y.T., Ma, W.F., Cui, H.F., 2002. Mineralization and tectonic setting of deephypabyssal granites in East Qinling molybdenumuntain. Mineral Deposits 21, 168–178 (in Chinese with English abstract).
Lu, Y.J., Loucks, R., Fiorentini, M., McCuaig, T.C., Evans, N., Yang, Z.M., Hou, Z.Q., Kirkland, C., Parra-Avila, L., Kobussen, A., 2016. Zircon compositions as a pathfinder for porphyry Cu ± Mo ± Au deposits. Society of Economic Geologists Special Publication No. 19 on Tethyan Tectonics and Metallogeny, pp. 329–347.
Ludwig, K.R., 2003. User's manual for Isoplot 3.0: A geochronological toolkit for Microsoft Excel. Berkeley Geochronology Center Special Publication, Berkeley, California, 1–71.
Maniar, P.D., Piccoli, P.M., 1989. Tectonic discrimination of granitoids. Geol. Soc. Am. Bull. 101, 635–643.
Mao, J.W., Xie, G.Q., Bierlein, F., Ye, H.S., Qu, W.J., Du, A.D., Pirajno, F., Li, H.M., Guo, B.J., Li, Y.F., Yang, Z.Q., 2008. Tectonic implications from Re–Os dating of Mesozoic molybdenum deposits in the East Qinling-Dabie orogenic belt. Geochim. Cosmochim. Acta 72, 4607–4626.
Mao, J.W., Pirajno, F., Xiang, J.F., Gao, J.J., Ye, H.S., Li, Y.F., Guo, B.J., 2011. Mesozoic molybdenum deposits in the east Qinling-Dabie orogenic belt: characteristics and tectonic settings. Ore Geol. Rev. 43, 264–293.
Martin, H., 1999. Adakitic magmas: modern analogues of Archaean granitoids. Lithos 46, 411–429.
Maughan, D.T., Keith, J.D., Christiansen, E.H., Pulsipher, T., Hattori, K., Evans, N.J., 2002. Contribution from mafic alkaline magmas to the Bingham porphyry Cu-Au-Mo deposit, Utah, USA. Miner. Deposita 37, 17–37.
Meinert, L.D., 1992. Skarns and skarn deposits. Geosci. Can. 19, 145–162.
Meinert, L.D., 1993. Igneous petrogenesis and skarn deposits. Geol. Assoc. Can. Spec. Pap. 40, 569–583.
Meinert, L.D., 1995. Compositional variation of igneous rocks associated with skarn deposits-chemical evidence for a genetic connection between petrogenesis and mineralization. In: Thompson J. F. H. (Ed.), Magmas, fluids, and ore deposits. Min. Assoc. Canada Short Course Series 23, pp. 401–418.
Meng, D.M., Wang, R.T., Wang, P., Dai, J.Z., Liu, K., Jiang, C., 2014. Study of characteristics and metallogenic mechanism of Lengshuigou copper–molybdenum deposit in Zhashui-Shanyang ore concentration area, Qinling orogeny, Shaanxi Province. Mineral Deposits 33, 833–846 (in Chinese withEnglish abstract).
Mengason, M.J., Candela, P.A., Piccoli, P.M., 2011. Molybdenum, tungsten and manganese partitioning in the system pyrrhotite–Fe–S–O melt–rhyolite melt: impact of sulfide segregation on arc magma evolution. Geochim. Cosmochim. Acta 75, 7018–7030.
Moyen, J.F., 2009. High Sr/Y and La/Yb ratios: the meaning of the "adakitic signature". Lithos 112, 556–574.
Myers, J., Eugster, H.P., 1983. The system Fe-Si-O: oxygen buffer calibrations to 1500K. Contrib. Mineral. Petrol. 82, 75–90.
Nadoll, P., Mauk, J.L., Leveille, R.A., Koenig, A.E., 2015. Geochemistry of magnetite from porphyry Cu and skarn deposits in the southwestern United States. Miner. Deposita 50, 493–515.
Pearce, J.A., Harris, N.B.W., Tindle, A.G., 1984. Trace element discrimination diagrams for the tectonic interpretation of granitic rocks. J. Petrol. 25, 956–983.
Pirajno, F., 2013. The Geology and Tectonic Settings of China's Mineral Depoists. Springer Verlag, Berlin 689 pp. ISBN 978-94-007-4443-1.
Pirajno, F., Zhou, T.F., 2015. Intracontinental porphyry and porphyry-skarn mineral systems in eastern China: scrutiny of a special case "made-in-China". Econ. Geol. 110, 603–629.
Qiu, J.T., Yu, X.Q., Santosh, M., Zhang, D.H., Chen, S.Q., Li, P.J., 2013. Geochronology and magmatic oxygen fugacity of the Tongcun molybdenum deposit, northwest Zhejiang, SE China. Miner. Deposita 48, 545–556.
Rapp, R.P., Watson, E.B., Miller, C.F., 1991. Partial melting of amphibolite/eclogite and the genesis of Archean trondjemites and tonalites. Precambrian Res. 51, 1–25.
Ren, T., Wang, R.T., Xie, G.Q., Li, J.B., Dai, J.Z., Guo, Y.H., Dang, K.F., Wu, X.Q., 2014. Geochemistry and rock-forming and ore-forming epochs of Chigou Cu porphyry deposit in Shaanxi Province, and their implications. Mineral Deposits 33, 807–820 (in Chinese with English abstract).

Richards, J.P., 2003. Tectono-magmatic precursors for porphyry Cu-(Mo-Au) deposit formation. Econ. Geol. 98, 1515–1533.
Richards, J.P., Spell, T., Rameh, E., Razique, A., Fletcher, T., 2012. High Sr/Y magmas reflect arc maturity, high magmatic water content, and porphyry Cu ± Mo ± Au potential: Examples from the tethyan arcs of central and eastern Iran and Western Pakistan. Econ. Geol. 107, 295–332.
Ripley, E.M., Brophy, J.G., Li, C., 2002. Copper solubility in a basaltic melt and sulfide liquid/silicate melt partition coefficients of Cu and Fe. Geochim. Cosmochim. Acta 66, 2791–2800.
Rollinson, H.R., 1993. Using Geochemical Data: Evaluation, Presentation, Interpretation. Longman Scientific and Technical Press, pp. 306–308.
Shaanxi Mineral Resources and Geological Survey. 2013. Achievement report of mineral resource potential evaluation for Shaanxi Province (in Chinese).
Söderlund, U., Patchett, P.J., Vervoort, J.D., Isachsen, C.E., 2004. The ^{176}Lu decay constant determined by Lu–Hf and U-Pb isotope systematics of Precambrian mafic intrusions. Earth Planet. Sci. Lett. 219, 311–324.
Stein, H.J., Markey, R.J., Morgan, J.W., Du, A.D., Sun, Y., 1997. Highly precise and accurate Re–Os ages for molybdenite from the East Qinling molybdenum belt, Shaanxi Province, China. Econ. Geol. 92, 827–835.
Sun, S.S., McDonough, W.F., 1989. Chemical and isotopic systematics of oceanic basalts: implications for mantle composition and processes. In: Magmatism in the Ocean Basins, Saunders, A.D., Norry, M.J. (Eds.), Geol. Soc. Lond. Spec. Publ. 42, pp. 313–345.
Sun, W.D., Liang, H.Y., Ling, M.X., Zhan, M.Z., Ding, X., Zhang, H., Yang, X.Y., Li, Y.L., Ireland, T.R., Wei, Q.R., Fan, W.M., 2013. The link between reduced porphyry copper deposits and oxidized magmas. Geochim. Cosmochim. Acta 103, 263–275.
Sun, W.D., Huang, R.F., Li, H., Hu, Y.B., Zhang, C.C., Sun, S.J., Zhang, L.P., Ding, X., Li, C.Y., Zartman, R.E., Ling, M.X., 2015. Porphyry deposits and oxidized magmas. Ore Geol. Rev. 65, 97–131.
Trail, D., Watson, E.B., Tailby, N.D., 2012. Ce and Eu anomalies in zircon as proxies for oxidation state of magmas. Geochim. Cosmochim. Acta 97, 70–87.
Vervoort, J.D., Blichert-Toft, J., 1999. Evolution of the depleted mantle: Hf isotope evidence from juvenile rocks through time. Geochim. Cosmochim. Acta 63, 533–556.
Wang, X.X., Wang, T., Jahn, B.M., Hu, N.G., Chen, W., 2007. Tectonic significance of Triassic lamprophyres from the North Qinling orogen. Geol. Magazine 144, 1–12.
Wang, R.T., Ren, T., Li, J.B., Dai, J.Z., Wang, D.S., Wang, Y.T., Yan, Z., 2010. Geochemical characteristics, metallogenetic model and exploration predicting of Yindongzi Ag-Pb polymetallic deposit, Zhashui County, Shaanxi Province, China. Acta Geol. Sin. 84 (3), 418–430 (in Chinese with English abstract).
Wang, X.X., Wang, T., Qi, Q.J., Li, S., 2011a. Temporal-spatial variations, origin and their tectonic significance of the Late Mesozoic granites in the Qinling, Central China. Acta Petrol. Sin. 27, 1573–1593 (in Chinese with English abstract).
Wang, X.X., Wang, T., Castro, A., Pedreira, R., Lu, X.X., Xiao, Q.H., 2011b. Triassic granitoids of the Qinling orogen, central China: genetic relationship of enclaves and rapakivi-textured rocks. Lithos 126, 369–387.
Wang, F.Y., Liu, S.A., Li, S.G., He, Y.S., 2013a. Contrasting zircon Hf–O isotopes and trace elements between ore-bearing and ore-barren adakitic rocks in central-eastern China: implications for genetic relation to Cu–Au mineralization. Lithos 156–159, 97–111.
Wang, L.J., Griffin, W.L., Yu, J.H., O'Reilly, S.Y., 2013b. U-Pb and Lu–Hf isotopes in detrital zircon from Neoproterozoic sedimentary rocks in the northern Yangtze Block: implications for Precambrian crustal evolution. Gondwana Res. 23, 1267–1272.
Wang, X.X., Wang, T., Ke, C.H., Yang, Y., Li, J.B., Li, Y.H., Qi, Q.J., 2015a. Nd-Hf isotopic mapping of late mesozoic granitoids in the East Qinling Orogen, Central China: constraint on the basements of terranes and distribution of Mo mineralization. J. Asian Earth Sci. 103, 169–183.
Wang, R.T., Wang, X.Y., Ren, T., Li, J.B., Meng, D.M., Dai, J.Z., Wang, T., Zhang, S.M., 2015b. Study on exploration methods combination for porphyry and skarn type metal ore deposit in the Zhashui-Shanyang concentration area. Acta Petrol. Sin. 31, 245–260 (in Chinese with English abstract).
Wang, S.W., Zhou, T.F., Yuan, F., Fan, Y., Zhang, L.J., Song, Y.L., 2015c. Petrogenesis of Dongguashan skarn-porphyry Cu-Au deposit related intrusion in the Tongling district, eastern China: geochronological, mineralogical, geochemical and Hf isotopic evidence. Ore Geol. Rev. 64, 53–70.
Wilkinson, J.J., 2013. Triggers for the formation of porphyry ore deposits in magmatic arcs. Nature Geosci. 6, 917–925.
Wu, F.F., Wang, Z.Q., Wang, T., Yan, Z., Chen, L., 2012. Shrimp zircons U-Pb ages and geochemical characteristics of the Banbanshan K-feldspar granite in Shanyang, South Qinling orogenic belt. J. Mineral. Petrol. 32 (2), 63–73 (in Chinese with English abstract).
Wu, F.F., 2013. Research on the magmatite and its metallogenic tectonic setting in the Shanyang–Zhanshui area, middle Qinling Orogenic belt. Dissertation for Doctoral degree. Chinese Academy of Geological Sciences, pp.1–183 (in Chinese with English abstract).
Wu, F.F., Wang, Z.Q., Yan, Z., Chen, L., Xia, C.L., Guo, Y.H., Peng, Y.M., 2014. Geochemical characteristics, zircons U-Pb ages and Lu-Hf isotopic composition of the Yanshanian intermediate-acidic plutons in the Shanyang-Zhashui areas, Qinling Orogenic Belt. Acta Petrol. Sin. 30, 451–471 (in Chinese with English abstract).
Xie, G.Q., Ren, T., Wang, R.T., Xian, C.L., Li, J.B., Da, J.Z., Gou, Y.H., Wang, C., 2012. MC–LA–ICPMS zircon U-Pb age of the ore-bearing igneous rocks for the Chigou Cu deposit in the Zhashan basin, Shanxi province and its geological implication. Acta Petrol. Sin. 28, 15–26 (in Chinese with English abstract).
Xie, G.Q., Mao, J.W., Wang, R.T., Ren, T., Li, J.B., Dai, J.Z., 2015. Origin of Late Mesozoic granitoids in the newly discovered Zha-Shan porphyry Cu district, South Qinling, central China, and implications for regional metallogeny. J. Asian Earth Sci. 103, 184–197.
Xie, G.Q., Mao, J.W., Wang, R.T., Meng, D.M., Sun, J., Dai, J.Z., Ren, T., Li, J.B., Zhao, H.J., 2017. Origin of the Lengshuigou porphyry-skarn Cu deposit in the Zha-Shan district, South Qinling, central China, and implications for differences between porphyry Cu and Mo deposits. Miner. Deposita 52, 621–639.
Xiong, X., Zhu, L.M., Zhang, G.W., Li, B., Qi, L., Stevenson, D., Yang, T., Wang, F., Zheng, J., Jiang, H., Guo, A.L., 2016. Geology and geochemistry of the Triassic Wenquan Mo deposit and Mo-mineralized granite in the Western Qinling Orogen, China. Gondwana Res. 30, 159–178.
Xu, J., Zheng, Y.Y., Sun, X., Shen, Y.H., 2016. Geochronology and petrogenesis of Miocene granitic intrusions related to the Zhibula Cu skarn deposit in the Gangdese belt, southern Tibet. J. Asian Earth Sci. 120, 100–116.
Yan, Z., Wang, Z.Q., Yan, Q.R., Wang, T., Guo, X.Q., 2012. Geochemical constraints on the provenance and depositional setting of the Devonian Liuling Group, East Qinling Mountains, Central China: implications for the tectonic evolution of the Qinling Orogenic Belt. J. Sediment. Res. 82, 9–20.
Yan, Z., Wang, Z.Q., Chen, L., Liu, S.W., Ren, T., Xu, X.Y., Wang, R.T., 2014. Tectono-magmatism and metallogeneses of Shanyang-Zhashui ore concentration area in Qinling Orogen. Acta Petrol. Sin. 30, 401–414 (in Chinese with English abstract).
Yang, Y.F., Li, N., Chen, Y.J., 2012. Fluid inclusion study of the Nannihu giant porphyry Mo-W deposit, Henan Province, China: implication for the nature of porphyry ore-fluid systems formed in continental collision regime. Ore Geol. Rev. 46, 83–94.
Yang, Y.F., Chen, Y.J., Pirajno, F., Li, N., 2015. Evolution of ore fluids in the Donggou giant porphyry Mo system, East Qinling, China, a new type of porphyry Mo deposit: evidence from fluid inclusion and H-O isotope systematics. Ore Geol. Rev. 65, 148–164.
Yao, L., Lü, Z.C., Zhao, C.S., Pang, Z.S., Yu, X.F., Yang, T., Li, Y.S., Liu, P., Zhang, M.C., 2017. Zircon U-Pb geochronological, trace element, and Hf isotopic constraints on the genesis of the Fe and Cu skarn deposits in the Qiman Tagh area, Qinghai Province, Eastern Kunlun Orogen, China. Ore Geol. Rev. 91, 387–403.
Yu, Y.F., Fei, G.C., Li, Y.G., Long, X.R., Tian, E.Y., Liu, G.Q., Lv, F.M., Hua, K.Q., 2016. Oxygen fugacity of intrusions from Lannitang porphyry copper deposit in Zhongdian island arc, Yunnan: implications for mineralizaiton. J. Mineral. Petrol. 36, 28–36 (in Chinese with English abstract).
Yuan, X.C., 1996. Velocity structure of the Qinling lithosphere and mushroom cloud model. Sci. China Ser. D 39, 235–244.
Yuan, H.L., Gao, S., Liu, X.M., Li, H.M., Günther, D., Wu, F.Y., 2004. Accurate U-Pb age and trace element determinations of zircon by laser ablation-inductively coupled plasma mass spectrometry. Geostand. Geoanal. Res. 28, 353–370.
Yuan, H.L., Gao, S., Dai, M.N., Zong, C.L., Günther, D., Fontaine, G.H., Liu, X.M., Diwu, C.R., 2008. Simultaneous determinations of U-Pb age, Hf isotopes and trace element compositions of zircon by excimer laser ablation quadrupole and multiple collector ICP-MS. Chem. Geol. 247, 100–118.
Zeng, Q.D., Liu, J.M., Qin, K.Z., Fan, H.R., Chu, S.X., Wang, Y.B., Zhou, L.L., 2013. Types, characteristics, and time–space distribution of molybdenum deposits in China. Int. Geol. Rev. 55, 1311–1358.
Zhai, M.G., Meng, Q.R., Liu, J., Hou, Q.L., Hu, S.B., Li, Z., Zhang, H.F., Liu, W., Shao, J.A., Zhu, R.X., 2004. Geological features of Mesozoic tectonic regime inversion in eastern North China and implication for geodynamics. Earth Sci. Front. 11, 285–297 (in Chinese with English abstract).
Zhan, H.Y., Li, Z.K., Wu, W.H., Li, J.W., 2019. Geological characteristics and origin of Daxigou SEDEX siderite deposit in Shaanxi Province. Mineral Deposits 38, 1–20 (in Chinese with English abstract).
Zhang, Q., Li, C.D., 2012. Granites: implications for continental geodynamics. Oceanpress 1–276 (in Chinese with English abstract).
Zhang, B.R., Chen, D.X., Li, Z.J., Gu, X.M., Jiang, J.Y., Hu, Y.K., Li, F.L., Guo, W.Y., Li, Y. C., 1989. Region geochemistry of Shanyang–Zhashui metallogenic belt, Shanxi Province. Press of China University of Geosciences, Wuhan, pp. 1–221 (in Chinese with English abstract).
Zhang, H.F., Luo, T.C., Li, Z.J., Zhang, B.R., 1994. Element abundances and geological significances of granitoids of Eastern Qinling. J. Mineral. Petrol. 14, 1–8 (in Chinese with English abstract).
Zhang, G.W., Meng, Q.R., Lai, S.C., 1995. Structure and tectonics of the Qinling Orogenic belt. Sci. China Ser. B 25, 994–1003.
Zhang, H.F., Zhang, B.R., Ling, W.L., Gao, S., Ouyang, J.P., 1997. Late Proterozoic crustal accretion of South Qinling: Nd isotopic study from granitic rocks. Geochimica 26, 16–24 (in Chinese with English abstract).
Zhang, G.W., Zhang, B.R., Yuan, X.C., Xiao, Q.H., 2001. Qinling Orogen Belt and Continental Dynamics. Science Press, Beijing, pp. 1–855 (in Chinese).
Zhang, C.L., Wang, T., Wang, X.X., 2008. Origin and tectonic setting of the Early Mesozoic granitoids in Qinling orogenic belt. Geol. J. China Univ. 14, 304–316 (in Chinese with English abstract).
Zhou, T.F., Wang, S.W., Fan, Y., Yuan, F., Zhang, D.Y., White, N.C., 2015. A review of the intracontinental porphyry deposits in the Middle-Lower Yangtze River Valley metallogenic belt, Eastern China. Ore Geol. Rev. 65, 433–456.
Zhou, Z.J., Mao, S.D., Chen, Y.J., Santosh, M., 2016. U-Pb ages and Lu-Hf isotopes of detrital zircons from the southern Qinling Orogen: implications for Precambrian to Phanerozoic tectonics in central china. Gondwana Res. 35 (4), 323–337.
Zhu, L.M., Zhang, G.W., Guo, B., Lee, B., Gong, H.J., Wang, F., 2010. Geochemistry of the Jinduicheng Mo-bearing porphyry and deposit, and its implications for the geodynamic setting in East Qinling, P.R. China. Chem. Erde-Geochem. 70, 159–170.